Geotech Geol Eng (2026) 44:37
https://doi.org/10.1007/s10706-025-03557-6

ORIGINAL PAPER

Dielectric Properties of Class 2 UGM Under Varying Moisture and Temperature at 2.45 GHz for Microwave Dry-Back Modelling

Gopoojithaa Athmarajah · Jeffrey Walker · Kaushal Kishore · Amir Tophel · Jayantha Kodikara

Received: 15 September 2025 / Accepted: 27 November 2025 / Published online: 11 December 2025

Abstract Unbound granular materials (UGMs) are essential components in road construction, particularly in the base and sub-base layers of pavements. After compaction, these layers undergo a dry-back process to reduce excess moisture before sealing, thereby minimising sealing aggregate embedment and rutting under traffic loading. Conventional dry-back methods for compacted UGMs rely on solar radiation, which is time-consuming and dependent on climatic conditions, often delaying construction schedules. Microwave technology could offer a rapid alternative, but its implementation in road construction requires a better understanding of the complex permittivity (dielectric properties) of UGMs to optimise energy absorption and heat generation during microwave dry-back. This study characterises the complex permittivity of Class 2 UGM as a function of volumetric moisture content (VMC) and temperature using a Modified Free-space Transmission technique. Measurements were conducted across frequencies from 300 kHz to 4.5 GHz at controlled temperatures between 20 and 90 °C. The observations were fitted using exponential regression models to predict dielectric behaviour at only 2.45 GHz, a frequency commonly used in industrial microwave applications. Regression models developed incorporating both VMC and temperature achieved good predictive accuracy ($R^2 > 0.8$). Results reveal the dielectric constant (ε_r') increased exponentially with VMC. In contrast, dielectric loss (ε_r'') decreased, an atypical trend likely reflecting the transition from bound to free water. Temperature effects were also notable, with higher temperatures reducing dielectric loss by decreasing dipolar relaxation. Sensitivity analysis indicated that VMC had a greater influence on ε_r' as compared to temperature, while both parameters contributed comparably to ε_r''. The proposed empirical model provides a practical tool for predicting energy absorption in compacted UGMs, offering key insight needed to optimise microwave-based dry-back methods in pavement construction.

Keywords Dielectric constant · Dielectric loss · Unbound granular materials · Modified free-space transmission measurement technique · Volumetric moisture content · Temperature

G. Athmarajah · J. Walker · K. Kishore · A. Tophel (✉) · J. Kodikara
ARC Industrial Transformation Research Hub (ITRH) – SPARC Hub, Dept. of Civil and Environmental Engineering, Monash University, Clayton Campus, Melbourne, VIC 3800, Australia
e-mail: amir.tophel@monash.edu

G. Athmarajah
e-mail: gopoojithaa.athmarajah@monash.edu

J. Walker
e-mail: jeff.walker@monash.edu

K. Kishore
e-mail: kaushal.kishore1@monash.edu

J. Kodikara
e-mail: jayantha.kodikara@monash.edu

Abbreviations

UGM	Unbound granular material
VMC	Volumetric moisture content (v/v) (%)
OMC	Optimum moisture content (w/w) (%)
MDD	Maximum dry density (kg/m^3)
MAE	Mean absolute error
R^2	Coefficient of determination
ε'_r	Dielectric constant
ε''_r	Dielectric loss
θ_v	Volumetric moisture content (v/v) (%)
T	Temperature (℃)
S_r	Degree of saturation (%)

1 Introduction

In civil engineering, road construction remains a critical domain where the mechanical and environmental performance of unbound granular materials (UGMs) plays a pivotal role in determining the longevity and functionality of granular pavement structures. UGMs, composed of crushed rock or gravel with an appropriate fraction of fines, are typically used in granular pavement construction. The moisture condition of these materials significantly affects their strength, stiffness, and compaction behaviour, thereby influencing overall pavement performance (Dutta et al. 2024; Dushmantha and Gallage 2025). Pore water within the voids of compacted UGMs governs matric suction and inter-particle bonding, which contribute to the overall stiffness and compaction effectiveness of the compacted layer (Sun et al. 2021). At optimum moisture content (OMC), a reduction in suction and effective stress facilitates particle rearrangement, resulting in increased densification and a higher dry density during compaction (Hilf 1956; Kodikara 2012). Conversely, moisture content beyond OMC reduces compaction efficiency due to increased air pressure caused by trapped air within the voids of compacted UGMs (Kodikara 2012). Therefore, UGMs are generally compacted at or near their OMC to achieve maximum dry density (MDD) for a given compaction effort (Tophel et al. 2022). However, high moisture levels after compaction may generate excessive pore water pressure within the voids under repeated or heavy traffic loads and reduce the strength or stiffness of the compacted granular layers (Austroads 2008). Loss of stiffness can reduce the load-bearing capacity and increase the risk of rutting and premature failure (Salour 2015; Sun et al. 2021; Asha et al. 2025). To mitigate these risks, the dry-back process, a crucial stage in road construction, involves reducing the moisture content of compacted, wet, unbound granular pavement layers to achieve the desired degree of saturation (S_r) before the sealing application. In current practice, the dry-back process relies on solar radiation, which is time-consuming and often leads to construction delays due to its dependence on climatic conditions (Athmarajah et al. 2023; Midgley 2008).

To address these limitations, microwave energy has been proposed as a promising drying alternative for accelerating the drying of wet compacted UGMs (Athmarajah 2025; Athmarajah et al., 2025). Microwave drying has been widely adopted in various industries, including food processing, pharmaceuticals, wood, agriculture, and mining, owing to its rapid and volumetric heating characteristics (Sethy et al. 2015; Yao et al. 2020; Gulisano and Gallego 2021; Khan et al. 2019). However, the effective implementation of microwave drying in road construction requires a fundamental understanding of the complex permittivity or dielectric behaviour of UGMs, which dictates their interaction with electromagnetic energy.

Dielectric properties refer to the ability of a material to store and dissipate electrical energy when subjected to an electromagnetic field. These properties are characterised by two main components: the real component (dielectric constant, ε'_r), which indicates the material's capacity to store energy, and the imaginary component (dielectric loss, ε''_r), which reflects the material's ability to dissipate energy as heat (Trigos et al. 2021; Metaxas and Meredith 1983). These properties are influenced by factors such as moisture content, temperature, applied frequency, density, composition and particle size distribution (Kabir et al. 2020; Nelson 1991; Abdulraheem et al. 2024). Characterising these dependencies is critical for optimising the microwave drying process and predicting its performance under varying field conditions.

While several permittivity models have been developed for various soils, only a limited number of models explicitly target pavement materials such as UGMs (Kishore 2023). Many of these models were developed for the time-domain reflectometry (TDR) and ground penetrating radar (GPR) applications to estimate the volumetric moisture content (VMC) of soils and UGMs (Kishore 2023; Muller 2016; Topp et al. 1980; Pepin et al. 1995; Malicki et al. 1996; Du

Table 1 Summary of existing permittivity models for different soils and UGMs (θ_v represents the volumetric moisture content)

Developed model		Application	Reference
Topp	$\varepsilon_r' = 3.03 + 9.3\theta_v + 146\theta_v^2 - 76.7\theta_v^3$	Mineral soils	(Topp et al. 1980)
	$\varepsilon_r' = 1.74 - 0.34\theta_v + 135\theta_v^2 - 55.3\theta_v^3$	Organic soils	
	$\varepsilon_r' = 3.55 + 38\theta_v + 84.1\theta_v^2 - 44.1\theta_v^3$	Glass beads	
Roth	$\varepsilon_r' = 2.87 - 11.1\theta_v + 276\theta_v^2 - 272\theta_v^3$	Mineral soils	(Roth et al. 1992)
	$\varepsilon_r' = 0.97 - 10.9\theta_v + 87.4\theta_v^2 - 28\theta_v^3$	Organic soils	
Dasberg and Hopmans	$\varepsilon_r' = 2.7 + 38.4\theta_v + 44\theta_v^2 - 48\theta_v^3$	Sandy and clayey loam	(Orangi 2019)
Schaap	$\theta_v = 0.136\sqrt{\varepsilon_r'} - 0.119$	Forest floor soils	(Schaap et al. 1996)
Jacobsen and Schjønning	$\theta_v = -7.01 \times 10^{-2} + 3.47 \times 10^{-2}\varepsilon_r' - 11.6 \times 10^{-4}\varepsilon_r'^2 + 18 \times 10^{-6}\varepsilon_r'^3$	Coarse sandy soils to sandy clay loam soils	(Jacobsen and Schjonning 1993)
Baran	$\theta_v = 6 \times 10^{-6}\varepsilon_r'^3 - 5.98 \times 10^{-4}\varepsilon_r'^2 + 2.3831 \times 10^{-2}\varepsilon_r' - 6.2164 \times 10^{-2}$	Unbound granular material	(Baran 1994)
Ekblad and Isacsson	$\theta_v = 3.06 \times 10^{-5}\varepsilon_r'^3 - 1.67 \times 10^{-3}\varepsilon_r'^2 + 3.58 \times 10^{-2}\varepsilon_r' - 0.1040$	Unbound granular material	(Ekblad and Isacsson 2007)
Muller	$\theta_v = 6 \times 10^{-6}\varepsilon_r'^3 - 5.56 \times 10^{-4}\varepsilon_r'^2 + 2.538 \times 10^{-2}\varepsilon_r' - 0.08758$	Unbound granular material	(Muller 2016)
Kishore	$\theta_v = -0.0065\varepsilon_r'^3 + 0.2004\varepsilon_r'^2 - 0.3287\varepsilon_r' - 0.9274$	Unbound granular material	Kishore et al. (2022)

et al. 2025). However, they often neglect the dielectric loss (ε_r''), due to its relatively small magnitude compared with the dielectric constant (ε_r'). Furthermore, the impact of temperature on dielectric properties has not been thoroughly explored, especially at temperatures exceeding 60 °C, which are typical in microwave drying processes. Table 1 summarises the mathematical formulations of various existing permittivity models developed for different soils and UGMs. Although a few models, such as those by Baran (1994), Ekblad and Isacsson (2007), Muller (2016), Kishore (2023) and Kishore et al. (2022), have been applied to pavement materials, they share the same limitations, reducing their suitability for simulating energy absorption and heat generation in compacted UGMs under microwave exposure. Furthermore, as shown in Table 1, the existing empirical models differ primarily in their fitting parameters based on soil type and correlate only the dielectric constant with VMC, without considering temperature effects. These observations highlight the need for a model that accounts for both ε_r' and ε_r'' as functions of moisture and temperature, forming the basis for the predictive model developed in this study.

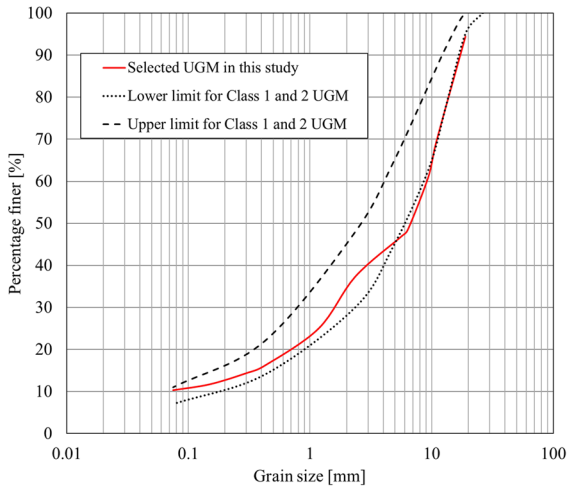

Fig. 1 Particle size distribution of selected unbound granular material (UGM) in this study

Several techniques are available to measure the dielectric properties of soils and granular materials, with each method suited to specific material types, frequency ranges, and application objectives. In laboratory environments, the open-ended coaxial probe method is one of the most commonly used techniques for characterising the complex permittivity of soils (Kabir et al. 2020; Palta et al. 2022). It enables measurement of both ε_r' and ε_r'' over a broad frequency range, but it requires close contact with the material surface and is best suited for homogeneous or powder samples (Skierucha et al. 2004; Vergnano et al. 2020). The resonant cavity method provides high measurement accuracy, particularly for low-loss materials within specific frequency range (typically 50–100 MHz), but its applicability is limited to small and uniform samples (Bircher et al. 2016). For larger or more heterogeneous samples, the free-space transmission method offers a non-contact alternative capable of operating over a wide frequency range (typically 3—100 GHz). This method allows for the measurement of flat, compacted specimens without requiring physical contact, which is particularly advantageous when testing materials at elevated temperatures or with rough or rigid surfaces (Muller and Scheuermann 2016; Wee et al. 2009; Ali et al. 2024). It also reduces the potential for measurement

Table 2 Geotechnical properties of selected UGM in this study

Property	Value	Standard
MDD modified [kg/m^3]	2345	AS-1289.5.2.1 (2017)
OMC modified [(w/w), %]	5.7	AS-1289.5.2.1 (2017)
Optimum degree of saturation [Sr_{opt}, %]	85	AS-1289.5.2.1 (2017)
Specific gravity [G_s, g/g]	2.78	AS-1289.3.5.1 (2006)
Liquid limit [LL, %]	22	AS-1289.3.1.1 (2009)
Plastic limit [PL, %]	17.5	AS-1289.3.1.1 (2009)
Plastic index [PI, %]	4.5	AS-1289.3.1.1 (2009)
Gravel [%]	55.7	AS-1289.3.6.1 (2009)
Sand [%]	34	AS-1289.3.6.1 (2009)
Fine content [< 0.075 mm, %]	10.4	AS-1289.3.6.1 (2009)

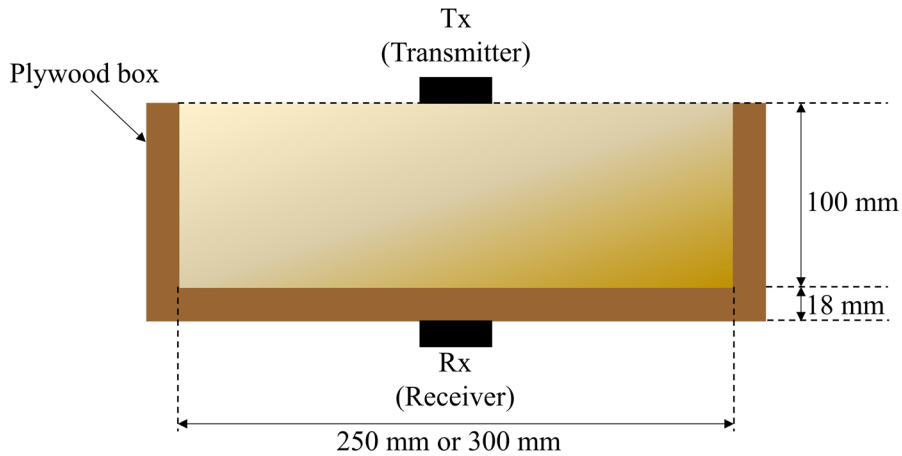

Fig. 2 Schematic representation of the simulated measurement setup showing the plywood sample box, transmitter (Tx) and receiver (Rx) configuration

disturbance, making it more appropriate for granular pavement materials compacted at field-representative densities.

To address the identified research gaps, this study aims to experimentally characterise the complex permittivity of compacted UGM as a function of volumetric moisture content and temperature using a modified free-space transmission method. Dielectric properties were measured over a broad frequency range (300 kHz–4.5 GHz) to capture the full response of the material. The results were used to develop empirical models for ϵ_r' and ϵ_r'' at 2.45 GHz, a frequency commonly used in industrial microwave applications. This model is essential, as it provides the dielectric input parameters for coupled electromagnetic, heat, and moisture simulations of microwave dry-back in UGM. Such simulations are needed to assess drying performance, estimate energy requirements, and optimise operational parameters such as power level, exposure time, and antenna configuration. Beyond simulation, the model also offers practical insights into how moisture and temperature affect dielectric behaviour, which is critical for designing field-scale microwave drying systems.

2 Methodology

2.1 Material Properties and Sample Preparation

Class 2 type UGM, the most common type of pavement material in Australia, and so typically used in constructing base and sub-base layers of roads, was selected for this study. The UGM, with a nominal maximum particle size of 20 mm, was supplied from the Boral Wollert Quarry located in Victoria, Australia. Figure 1 shows the particle size distribution of the selected UGM determined using a combination of wet and dry sieving in accordance with AS-1289.3.6.1 (2009). Following VicRoads guidelines (VicRoads 2017), the upper and lower limits for Class 1 and 2 UGMs are shown as dashed lines in Fig. 1. Key geotechnical properties of the selected UGM are outlined in Table 2.

2.2 Design and Selection of Sample Box for Dielectroscopy Measurements

To ensure the accuracy of permittivity measurements, careful consideration was given to the selection of an appropriate sample box size. The geometry of the sample box plays a critical role in influencing the propagation and reflection of electromagnetic waves during the measurements. Finite-difference time-domain (FDTD) simulations were performed using the GPRMax 2D software to evaluate the impact of box dimensions. Two empty wooden box configurations with internal dimensions of 250 mm × 250 mm × 100 mm and 300 mm × 300 mm × 100 mm were modelled under identical conditions as shown in Fig. 2. The geometry of the sample box was chosen based on findings from previous dielectric measurement studies reported in the literature, as well as practical considerations for easy manual handling of the compacted specimens (Muller and Scheuermann 2016; Kishore 2023).

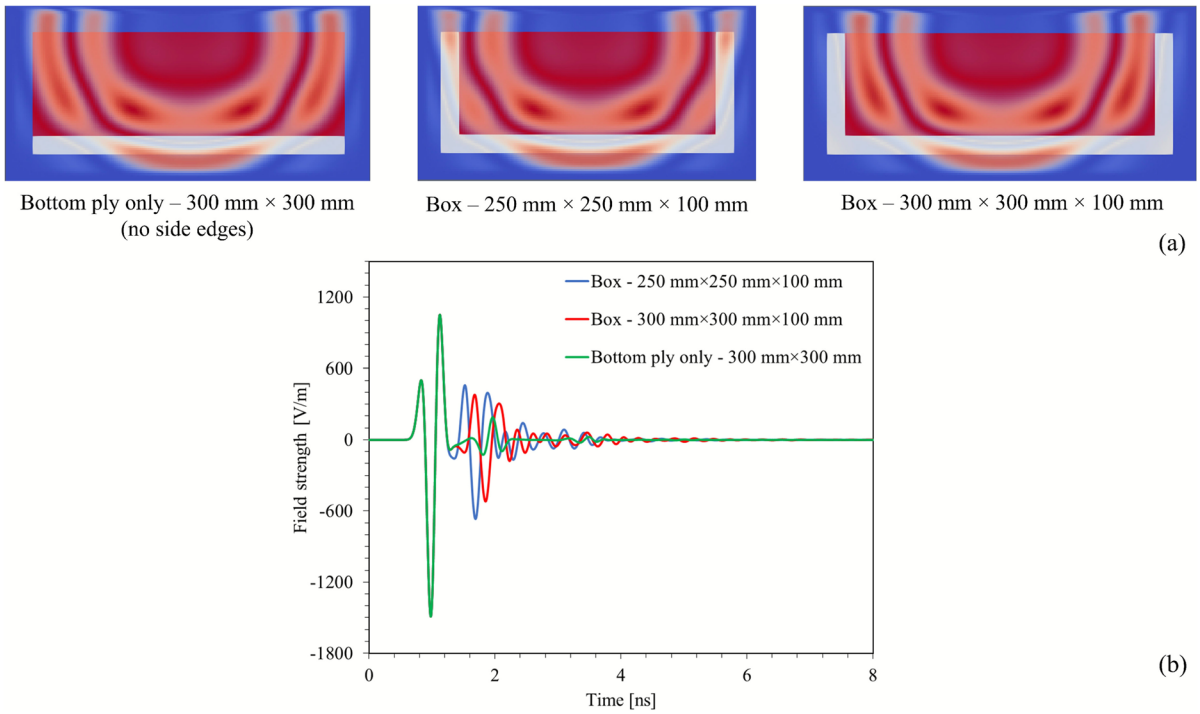

Fig. 3 Simulation results illustrating the influence of box dimensions on electromagnetic wave behaviour: **a** Field distribution snapshots for three different configurations, and **b** Corresponding field strength recorded at the receiver as a function of time

The 2D simulation domain consisted of the plywood sample box and surrounding air, with material properties assigned as $\varepsilon_r' = 1$ for air and $\varepsilon_r' = 2.5$ for the plywood walls. A 2.45 GHz Ricker wavelet was used as the excitation source, and the transmitter and receiver were positioned to match the experimental setup. All boundaries employed GPRMax's recursive integration complex-frequency-shifted perfectly matched layer (RIPML), which provides an efficient media-agnostic absorbing boundary condition and prevents artificial reflections from the model edges.

Figure 3 shows the temporal variation of the field strength recorded at the receiver. The results demonstrated that a sample box with dimensions of 250 mm × 250 mm × 100 mm was unsuitable for dielectric measurements, as reflections from the sidewalls and a double reflection from the base arrived nearly simultaneously, overlapping with the direct wave and compromising the clarity of the reference signal. On the other hand, the 300 mm × 300 mm × 100 mm box provided slightly improved temporal separation between the direct wave and subsequent reflections from sidewalls and the bottom surface, reducing unwanted reflections. Additionally, modelling the reference condition using only a 300 mm × 300 mm plywood sheet (no side edges) showed a substantial reduction in spurious reflections compared to an empty box.

These findings indicated that increasing the box size from 250 mm × 250 mm × 100 mm to 300 mm × 300 mm × 100 mm improved the temporal separation between the direct and reflected signals,

Table 3 Summary of initial volumetric moisture contents and achieved dry densities of compacted UGM samples used in complex permittivity measurements

Sample no	Initial volumetric moisture content [%]	Dry density [kg/m^3]	% Deviation from maximum dry density
1	13.7	2340.0	0.21
2	13.6	2339.6	0.23
3	11.9	2321.1	1.02
4	9.3	2275.2	2.98
5	4.0	2321.1	1.02
6	0.3	2275.2	2.98

thereby enhancing the clarity of the reference waveform (Fig. 3). Although larger box dimensions could potentially further reduce boundary reflections, their increased sample weight (around 30 kg) would make manual handling difficult. The chosen 300 mm × 300 mm × 100 mm configuration, therefore, represents an appropriate balance between minimising side-wall reflections and maintaining a manageable sample size. In addition, this box volume allows the material to be compacted to dry densities between 2100 and 2300 kg/m3, producing a sample mass of approximately 20–23 kg, which is practical for manual handling during repeated measurements. Hence, the 300 mm × 300 mm × 100 mm box was adopted for all dielectric property measurements.

2.3 Sample Preparation

The UGM selected for this study was oven-dried at 105°C for 24 h. Subsequently, the dried UGM was mixed with water (OMC) and then compacted inside the wooden mould in two layers using a modified Proctor hammer (4.9 kg), with 650 drops applied to each layer. The study by Kishore (2023) demonstrated

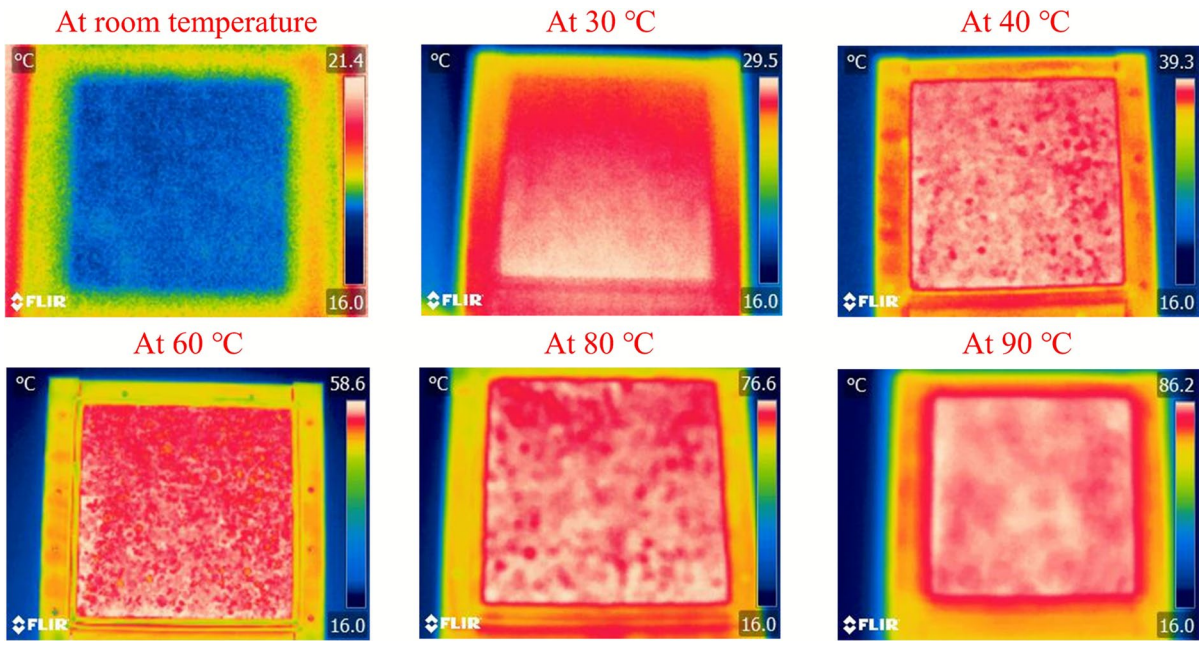

Fig. 4 Representative infrared (IR) thermal images of the compacted UGM sample at each target temperature (room temperature, 30 °C, 40 °C, 60 °C, 80 °C and 90 °C)

Table 4 Summary of surface temperature statistics extracted from IR thermal images, including maximum (Tmax), minimum (Tmin) and the resulting surface temperature variation (ΔT), at each target temperature

Target temperature [℃]	Maximum surface temperature observed [T_{max}, ℃]	Minimum surface temperature observed [T_{min},℃]	Difference [$\Delta T = T_{max} - T_{min}$,℃]
20	18.9	17.6	1.3
30	29.5	27.1	2.4
40	39.3	7.3	2.0
60	58.6	54.2	4.4
80	76.6	71.6	5.0
90	86.2	80.1	5.4

that density has a weak correlation with the complex permittivity of UGMs (correlation coefficient of 0.17), whereas volumetric moisture content exhibited a strong positive correlation with a correlation coefficient of 0.92. Therefore, the effect of density was not considered in this study. Instead, all measurements were conducted at a constant dry density, the maximum dry density (MDD), to reflect field-compacted conditions used in pavement construction.

Six UGM samples were first compacted at OMC to achieve MDD and were subsequently air-dried for several days to obtain different initial moisture contents for testing. This approach was intended to increase the compaction effectiveness at OMC and maintain similar density throughout the experimental period. A summary of initial conditions, including volumetric moisture content and dry density for each sample, is provided in Table 3. Each sample, representing a specific initial moisture level, was then tested at multiple temperature levels (room temperature, 30°C, 40°C, 60°C, 80°C, 90°C). After each permittivity measurement, samples were tightly wrapped and sealed with aluminium foil to minimise moisture loss. The samples were then kept in an oven for at least two days to increase their temperature incrementally to the specified temperature. The upper limit of 90 °C was selected to avoid the phase change of pore water at atmospheric pressure, which may cause rapid moisture loss, making it difficult to maintain steady-state conditions for accurate dielectric property determination.

Before each dielectric measurement, the gravimetric moisture content of the sample was determined by weight to account for any potential moisture loss during heating. Despite the precautions taken to minimise moisture losses during each measurement, difficulties in maintaining the initial moisture content caused slight variations (approximately 4 to 5% of the initial moisture content) from initial moisture contents when subjected to varying temperatures. Thermal images were captured using an infrared (IR) thermal imaging camera to ensure that the sample reached the target temperature. Measurements were taken soon after the samples were taken out of the oven to minimise their exposure to the environment and prevent any

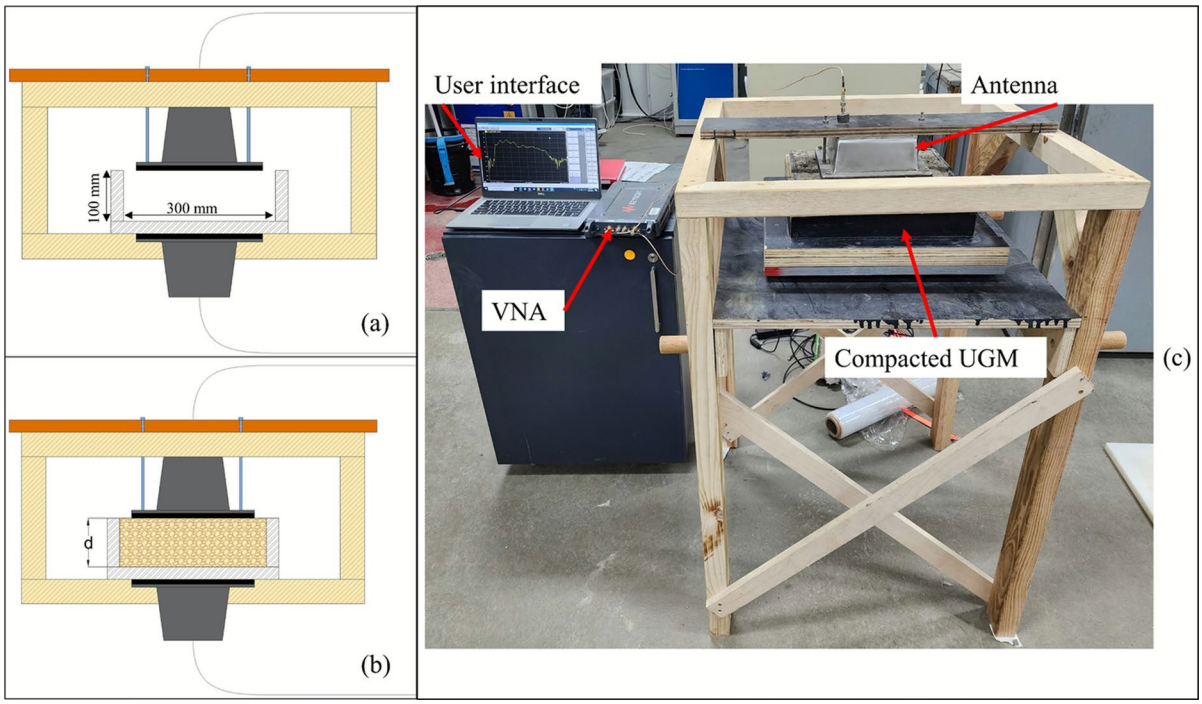

Fig. 5 Illustration of the experimental setup for the Modified free-space transmission method **a** Reference measurement with empty plywood box, **b** UGM sample characterisation, and **c** Photo of the experimental arrangement

significant temperature reduction. Representative IR images for each temperature level are presented in Fig. 4. The maximum (T_{max}) and minimum (T_{min}) surface temperatures extracted from these images were used to quantify the variation in surface temperature ($\Delta T = T_{max} - T_{min}$), as summarised in Table 4. These variations were small at lower temperatures ($\Delta T \approx 1$—2.4 °C at 20—40 °C) and increased at elevated temperatures ($\Delta T \approx 4$—5 °C at 60—90 °C). The larger ΔT values at elevated temperatures indicate increased thermal variability at higher heating levels. Although the IR measurements captured only the surface temperature distribution, the observed variation in Fig. 4 provides a reasonable indication of the thermal uniformity.

2.4 Measurement Technique of Complex Permittivity of UGM

A modified free-space transmission measurement technique (Fig. 5) was used to determine the dielectric properties of UGM over a range of frequencies from 300 kHz to 4.5 GHz. The modified free-space transmission measurement technique enables a non-destructive estimation of complex permittivity by measuring the relative changes in phase and amplitude of electromagnetic signals passing through a dielectric material with a known thickness placed in between two antennas (Muller and Scheuermann 2016). Generally, these measurements are determined from obtained scattering parameters (S-parameters) using a vector network analyser (VNA) before and after the insertion of the sample. S-parameters are denoted as S_{mn}, where, m and n are the receiving and transmitting ports of the VNA, respectively. The S-parameters such as input reflection coefficient (S_{11}), forward transmission coefficient (S_{21}), reverse transmission coefficient (S_{12}) and output reflection coefficient (S_{22}) were obtained using a two-port VNA in this study. The real (ε_r') and imaginary (ε_r'') components of the complex permittivity for low-loss materials can be obtained using

$$\varepsilon_r' \approx \left(1 + \frac{\Delta\Phi\lambda_0}{360d}\right)^2 \quad (1)$$

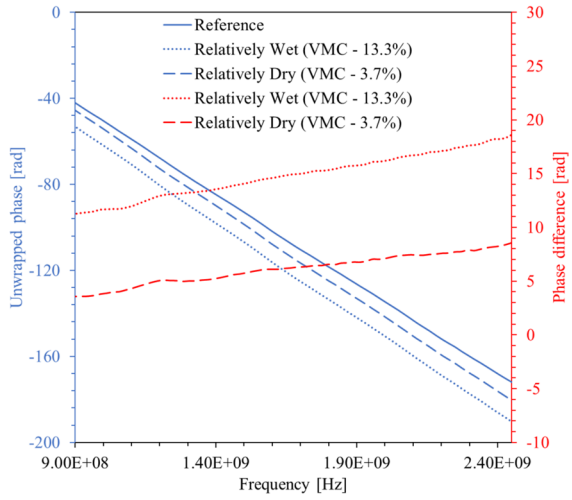

Fig. 6 Unwrapped phase signals and phase differences measured for relatively wet and dry UGM samples at 30 °C. Reference indicates measurements taken with an empty wooden box (i.e., without a UGM sample)

$$\varepsilon_r'' \approx \frac{\Delta A \lambda_0 \sqrt{\varepsilon'}}{8.686\pi d} \quad (2)$$

where $\Delta\Phi$ is the measured phase shift in degrees, λ_0 is the free space wavelength (m), d is the material thickness (m), and ΔA is the attenuation due to the insertion of the sample (dB). Equations (1) and (2) require both phase (degrees) and amplitude (dB) components of S_{21}, therefore the S-parameter S_{21} was obtained to estimate the complex permittivity of the UGM in this study.

Before starting the measurements, the VNA was calibrated using the Short, Open, Load, Thru (SOLT) technique (Keysight Technologies 2021). After calibration, measurements were taken using materials with known permittivity values (i.e., water at room temperature and Teflon) to ensure the accuracy of complex permittivity measurements of UGM using a modified free-space transmission measurement technique. The results showed that both the dielectric constant and dielectric loss of permittivity remained consistent with theoretical values within the frequency range of 1 GHz to 2.75 GHz, confirming this range as the stable operating window. Detailed calibration results are provided in Appendix A.

After comparing the measured permittivity values with the known permittivity values of water

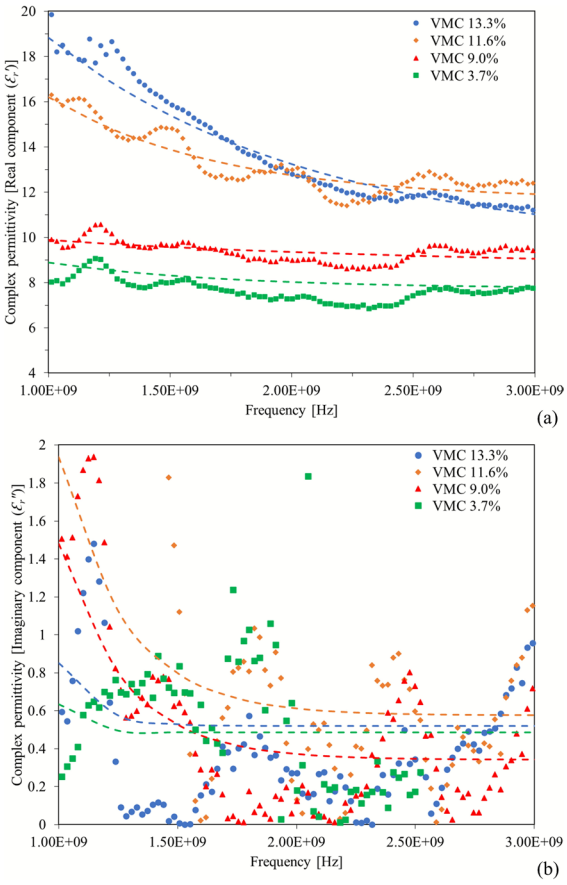

Fig. 7 Complex permittivity of UGM at 30°C and different moisture contents: **a** dielectric constant and **b** dielectric loss (VMC–volumetric moisture content, Dashed lines represent the fitted curve, and points represent the measured data)

and Teflon, a systematic approach was employed to measure the complex permittivity of the UGM. Initially, a reference signal S_{21} was ascertained within a wooden box without any samples, as exhibited in Fig. 5a. Subsequently, S_{21} parameters were retrieved for the compacted UGM sample within the wooden box (Fig. 5b). The acquired parameters were analysed, where the phase values were unwrapped to ascertain the true signal delay through the samples. Phase unwrapping is a signal processing technique used to reconstruct the true phase shift of a wave by correcting discontinuities caused by wrapping. Since phase values are typically measured within a range of $-\pi$ to $+\pi$ (or $-180°$ to $+180°$), abrupt jumps can occur when the phase exceeds these limits. The unwrapping process removes these artificial jumps by adding or subtracting integer multiples of 2π, thereby producing a continuous phase profile (Kaplan and Ulrych 2007; Gdeisat and Lilley 2011). This step is crucial for accurately estimating the time delay of electromagnetic waves as they pass through the material. Figure 6 depicts the material response in terms of unwrapped phase and phase change for representative moisture conditions namely relatively dry and relatively wet states. The selected moisture contents in Fig. 6 represent the upper (13.3%) and lower (3.7%) bounds of the test range at 30 °C, allowing for a clear comparison of dielectric response between contrast moisture conditions. Furthermore, the positions of the transmitting and receiving antennas were kept fixed throughout the experiment to eliminate any phase shift ambiguity.

Following the measurement of complex permittivity, the data were analysed to establish empirical relationships between VMC, temperature, and dielectric parameters. Exponential regression models were subsequently developed to predict the ε_r' and ε_r'' at 2.45 GHz. The frequency of 2.45 GHz was selected for analysing the complex permittivity of UGM, as this frequency is commonly used in both industrial and laboratory microwave drying processes and lies within the stable calibration window (Khan et al. 2019; Kumar et al. 2017; Shen et al. 2020). The averaged permittivity values corresponding to each VMC-temperature combination were used for model fitting (Sect. 3.2), and the predictive accuracy of the regression was evaluated using the coefficient of determination (R2) and mean absolute error (MAE). A subsequent sensitivity analysis was also performed to quantify the relative influence of VMC and temperature on the ε_r' and ε_r'' of the selected UGM (Sect. 3.5).

3 Results and Discussion

3.1 Complex Permittivity of UGM

Figure 7 presents the dielectric constant (ε_r') and dielectric loss (ε_r'') of UGM at 30°C with different VMCs in the frequency range from 1 to 3 GHz. The ε_r' values exhibit a clear decreasing trend with increasing frequency and decreasing VMC. This inverse relationship with frequency follows a non-linear (exponential) pattern at each moisture content level, indicating the complex interaction between the

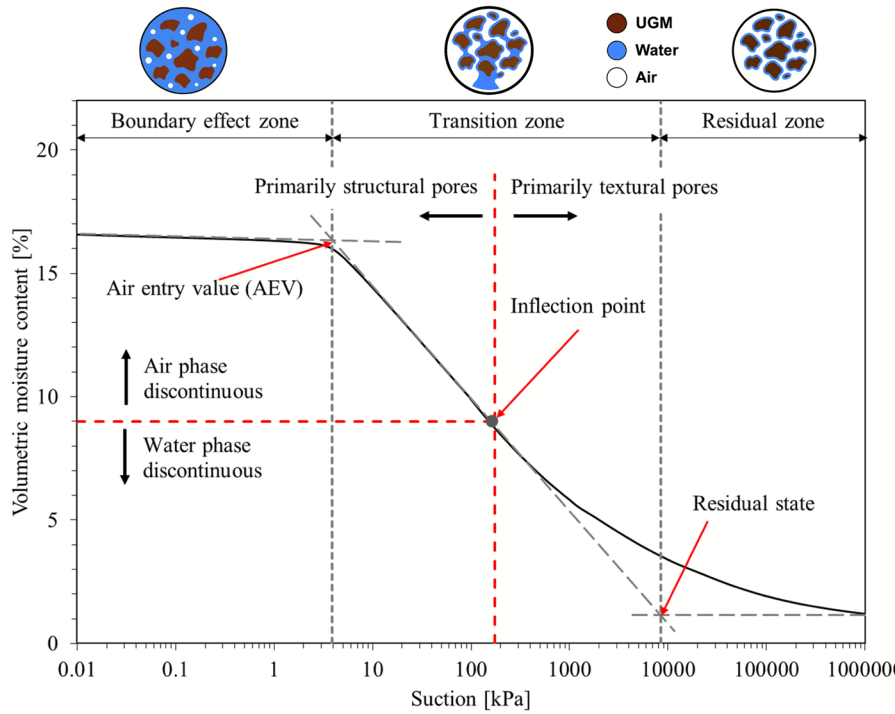

Fig. 8 Soil Water Retention curve (SWRC) for Class 2 UGM used in this study, illustrating the continuity and discontinuity of the water and air phases within different zones. These include: the **boundary effect** zone, where most pores remain filled with water, the **transition zone**, where large changes in VMC occur with small changes in suction and the inflection point (~8.9% VMC) marks the onset of continuity of air and water phases; and the **residual zone**, where water is tightly bound in textural pores

electromagnetic waves and the material. The ε_r'' variations depicted in Fig. 7b, also show a similar decreasing trend with increasing frequency and decreasing VMC. However, ε_r'' data exhibit noticeable variability relative to ε_r'. This behaviour is consistent with previous dielectric studies on UGMs measured at room temperature (Kishore 2023; Müller et al. 2012) and reflects the sensitivity of the ε_r'' to measurement noise or the inherent heterogeneity of UGMs. Temperature fluctuations in the specimen and the surrounding air may have further contributed to the scatter observed in ε_r'' readings (Fig. 7b).

Figure 7 also indicates that the dielectric properties of UGM (ε_r') exhibit a notable increase after reaching a 9% volumetric moisture content. This phenomenon can be explained using the Soil Water Retention Curve (SWRC) for the tested material (Fig. 8), which describes the relationship between the moisture content and matric suction of unsaturated soils, providing insight into how water can be retained within the pore structure under varying suction conditions (Fredlund 2006; Fazel Mojtahedi et al. 2024). As shown in Fig. 8, the SWRC for unsaturated soils and UGMs is typically divided into three distinct zones: boundary effect zone, transition zone and residual zone (Fredlund 2006; Azoor et al. 2019). In the boundary effect zone, water is held by capillary forces within structural pores, where the air phase is occluded, allowing relatively free water movement. In contrast, the residual zone contains tightly bound water (below residual state VMC) held by physicochemical forces in textural pores, making it largely immobile (Saarenketo 1998). Between these two zones lies the transition zone, characterised by the largest changes in moisture content for a given change in suction. The inflection point within this zone represents the VMC or suction at which both water and air phases are continuous, marking the shift in dominant pore drainage mechanisms (Azoor et al. 2019).

The SWRC for the tested material, shown in Fig. 8, identifies the inflection point at approximately 8.9% VMC, which corresponds to the onset of free water availability. An increase in VMC from the residual state gradually increases the dielectric properties of UGM due to the limited contribution of bound water to polarisation. However, beyond the inflection point, the higher mobility of free water molecules within the interconnected structural pores leads to a sharper rise in dielectric properties (refer Fig. 7). This behaviour reflects the dominant influence of free water on the material's electromagnetic response, as free water

Table 5 Summary of the number of replicate measurements collected under each volumetric moisture content-temperature combination

Volumetric moisture content [VMC, %]	Temperature [°C]	Number of replicates
13.6	20	3
13.5	30	3
5.7	40	3
4.6	60	3
1.5	80	3
0.3	90	4
13.7	20	3
13.3	30	3
12.8	40	3
11.9	60	4
10.1	80	5
7.1	90	4
11.6	30	6
11.3	40	6
10.0	60	7
8.5	80	7
6.7	90	7
4	20	6
3.7	30	6
3.1	40	7
2.3	60	7
9.3	20	6
9	30	7
8.6	40	7
7.9	60	7
5.7	80	8
4	90	7
0.3	20	7
0.1	40	7
0.1	60	7
0.1	80	7

is more polarisable and contributes substantially to changes in the dielectric properties of UGM. In the lower frequency range (below 100 MHz), ionic conduction is the dominant mechanism of electric field dispersion, while at microwave frequencies (above 1 GHz), dipolar relaxations become more significant (Athmarajah et al. 2024). As a result, at these frequencies (1 GHz—3 GHz), microwave energy absorption by water is predominant, leading to higher dielectric properties at higher moisture contents due to the transition from bound to free water.

3.2 Regression Model for UGM at 2.45 GHz Frequency

This section presents the development of a regression model to describe the complex dielectric permittivity of compacted Class 2 UGM as a function of volumetric moisture content and temperature at 2.45 GHz, which represents the standard industrial microwave frequency used in heating and drying applications.

To ensure the reliability and accuracy of the regression model at 2.45 GHz, the following data processing approach was adopted. For each combination of VMC and temperature, multiple permittivity measurements were obtained under the same conditions using the modified free-space transmission method. As presented in Fig. 7 from the previous section, a representative set of frequency-dependent measurements was used to illustrate the general trend. For the regression model, the permittivity values at 2.45 GHz were extracted from these repeated measurements. For the 31 distinct VMC-temperature combinations tested in this study, the number of replicate measurements collected under each condition is summarised in Table 5.

Due to the observed variability, particularly in the dielectric loss (ε_r''), a screening process was conducted to remove extreme outlier values. These outlier points were identified based on their significant deviation from surrounding values and reference values reported in the literature for UGMs. For each VMC-temperature condition, the mean ($\bar{x}$) and standard deviation (σ) of ε_r' and ε_r'' were computed from the replicate measurements. A replicate was classified as an outlier when either its real or imaginary component deviated from the mean by more than two standard deviations, as

$$Deviation = x_i - \bar{x} > 2\sigma \tag{3}$$

where x_i is the individual replicate value. Replicates exceeding this threshold were removed, and the remaining values were then averaged to obtain representative dielectric constant and dielectric loss values, along with their corresponding standard deviations ($\pm 1\,\sigma$) to reflect experimental variability.

Table 6 Estimated coefficients and ± 95% confidence intervals for exponential regression model at different temperatures (MAE-Mean Absolute Error)

		20°C	30°C	40°C	60°C	80°C	90°C
Dielectric constant (ε_r')	A'	2.90 ± 0.77	3.02 ± 1.28	2.70 ± 0.94	2.05 ± 1.07	2.03 ± 1.90	1.50 ± 0.69
	B'	2.89 ± 0.62	3.15 ± 0.97	3.34 ± 0.46	3.35 ± 0.74	3.37 ± 1.11	1.27 ± 0.40
	C'(%)	12.32 ± 1.18	12.88 ± 2.76	10.71 ± 1.36	11.05 ± 2.87	11.46 ± 2.66	8.59 ± 1.67
	R^2	0.99	0.89	0.97	0.96	0.99	0.87
	MAE	0.21	0.67	0.68	0.61	0.37	0.52
Dielectric loss (ε_r'')	A''	1.26 ± 0.09	1.06 ± 0.77	0.98 ± 0.18	0.77 ± 1.30	0.80 ± 0.30	0.59 ± 4.83
	B''	0.04 ± 0.05	0.06 ± 0.15	0.10 ± 0.13	0.10 ± 0.33	0.12 ± 0.27	0.11 ± 4.78
	C''(%)	4.76 ± 1.82	5.42 ± 0.48	6.31 ± 2.69	6.96 ± 2.17	7.28 ± 3.27	2.09 ± 1.31
	R^2	0.98	0.90	0.98	0.90	0.99	0.31
	MAE	0.04	0.09	0.05	0.07	0.04	0.01

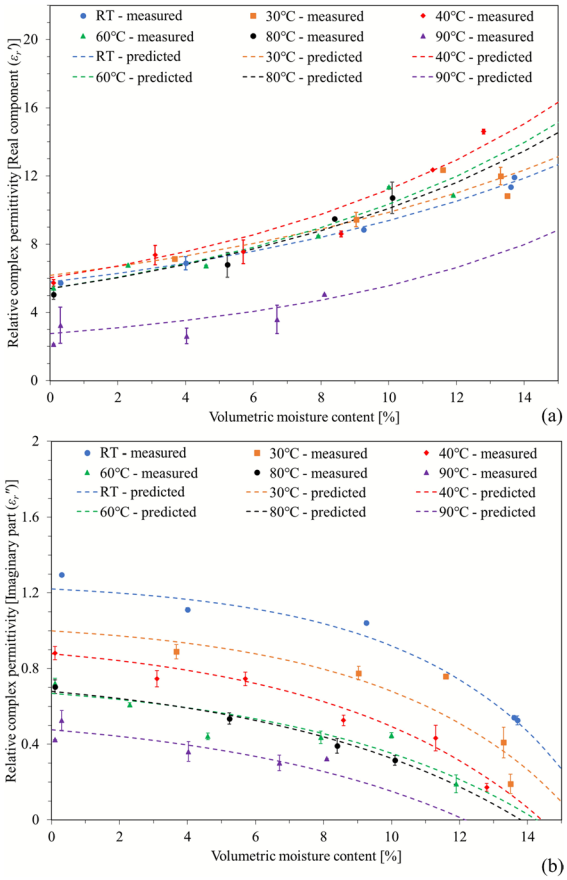

Fig. 9 Complex permittivity of Class 2 UGM at 2.45 GHz frequency, different volumetric moisture contents and temperatures **a** dielectric constant and **b** dielectric loss (RT- room temperature ~ 20°C). Error bars represent ± 1 standard deviation

Table 7 Temperature-dependent models and fitted parameters with their 95% confidence intervals for regression coefficients A', B', C', A'', B'', and C'' [T- temperature (°C)]

Coefficient	Model	Parameter	Fitted model	R^2
A'	$a_1' \times T + a_0'$	a_0'	3.42 ± 0.5	0.92
		a_1'	-0.02 ± 0.01	
B'	$b_0' - b_1' e^{\left(\frac{T}{b_2'}\right)}$	b_0'	3.00 ± 0.91	0.73
		b_1'	0.0004 ± 0.01	
		b_2'	11.08 ± 2.07	
C'(%)	$c_1' \times T + c_0'$	c_0'	13.34 ± 2.84	0.58
		c_1'	-0.04 ± 0.05	
A''	$a_1'' \times T + a_0''$	a''_0	1.34 ± 0.22	0.90
		a''_1	-0.01 ± 0.003	
B''	$b_0'' - b_1'' e^{\left(-\frac{T}{b_2''}\right)}$	b''_0	0.12 ± 0.08	0.93
		b''_1	0.21 ± 0.10	
		b''_2	20.47 ± 3.69	
C''(%)	$c_1'' \times T + c_0''$	c''_0	4.46 ± 1.47	0.88
		c''_1	0.04 ± 0.09	

Table 8 Summary of the dataset division and validation settings used for model validation

Total number of data points	31
Training dataset size	80% of the full dataset (n = 25)
Testing dataset size	20% of the full dataset (n = 6)
Validation method	k-fold cross-validation
Number of folds	5

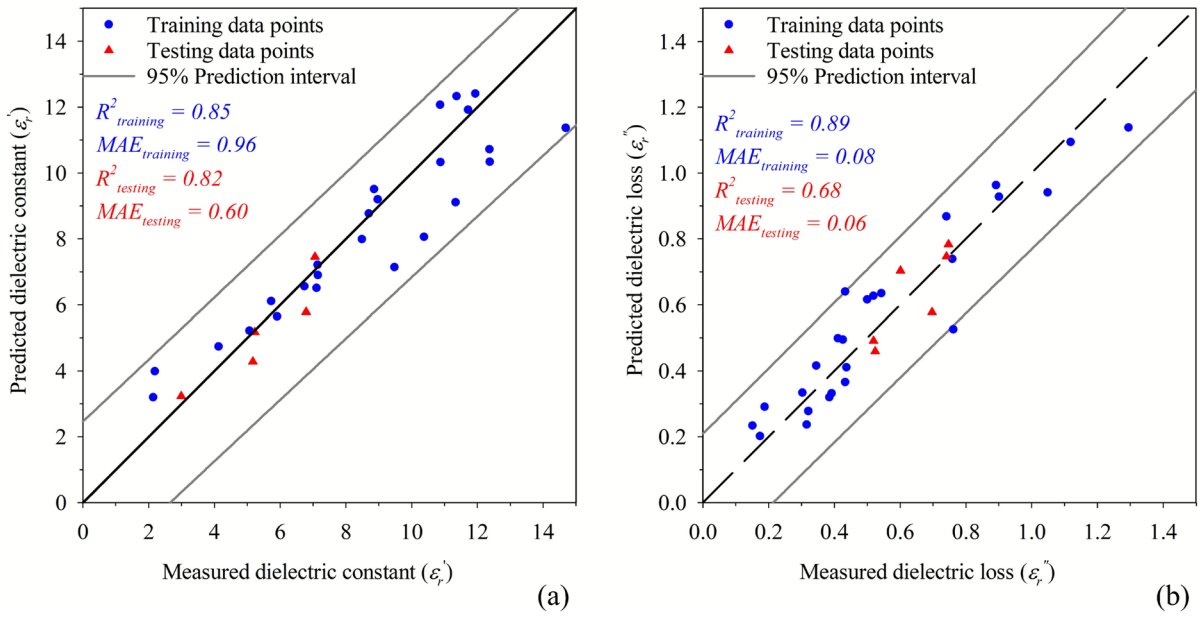

Fig. 10 Comparison of the developed regression model's dielectric properties prediction with measured dielectric properties for **a** dielectric constant (ε_r') and **b** dielectric loss (ε_r''). The black dashed indicates the 1:1 line, and the grey solid lines represent the 95% prediction interval

To model the variation of dielectric constant and dielectric loss with respect to VMC at different temperatures, exponential regression models were fitted to the measured values. The general form of the fitted model for the complex permittivity of UGM was assumed as

$$\varepsilon_r' = A' + B' e^{\left(\frac{VMC}{C'}\right)} \tag{4}$$

$$\varepsilon_r'' = A'' - B'' e^{\left(\frac{VMC}{C''}\right)} \tag{5}$$

where A', B', and C' are coefficients for dielectric constant, A'', B'', and C'' are coefficients for dielectric loss that are functions of temperature, as shown in Table 6, and VMC is the volumetric moisture content (%). The coefficients in Table 6 show that the exponential model achieved consistently high R^2 values (>0.8) for both ε_r' and ε_r'' across the tested temperature range, confirming a strong correlation between measured and fitted values. The lower R^2 value at 90 °C indicates greater variability in the dielectric loss data at elevated temperatures. This behaviour might be attributed to the reduced stability of measurements under higher temperatures. The wider confidence intervals at 80 °C and 90 °C, particularly for the dielectric loss coefficients, further indicate increased variability and reduced parameter stability at elevated temperatures.

The variations of complex permittivity of a Class 2 UGM at 2.45 GHz frequency, with different volumetric moisture contents and temperatures, are shown in Fig. 9. The data points represent measured values, while the dashed lines represent the model predictions. The fitted models demonstrate a good agreement with experimental values across different temperatures and moisture levels. Building upon the regression models for dielectric constant and dielectric loss at various temperatures, the analysis was extended to develop a comprehensive model that incorporates both volumetric moisture content and temperature. The coeficients A', B', C', A'', B'', and C'' were modeled as functions of temperature, as summarised in Table 7 and combined with the fitted exponential regression model for dielectric constant (Eq. (4)) and dielectric loss (Eq. (5)) of a Class 2 UGM. The fitted temperature-dependent models in Table 7 show generally stable parameter trends with temperature ($R^2 > 0.7$).

The coefficients incorporating both volumetric moisture content and temperature effects (Eqs. (4) and (5), and Table 7) were then used to generate the combined regression model. The predicted values of dielectric constant and dielectric loss were compared against the measured data to evaluate the model's predictive capability. To validate the models, the full dataset was randomly divided into training (80%) and testing (20%) subsets. A summary of the dataset division and validation settings is provided in Table 8. The model performance was assessed by comparing predicted values against the measured data, and quantified using the coefficient of determination (R^2) and mean absolute error (MAE). The results shown in Fig. 10 demonstrate a good agreement ($R^2 > 0.8$) between predicted and measured values, confirming the robustness and predictive accuracy of the combined regression models.

The variations in dielectric constant or real component (ε_r') of the complex permittivity increase with increasing moisture contents for all temperatures (Fig. 9a). This indicates that the presence of more free water molecules substantially contributes to the increased dielectric constants at higher volumetric moisture contents (Taheri et al. 2018). The dielectric constants of Class 2 UGM at 2.45 GHz frequency also exhibited a notable dependence on temperature. It can be observed in Fig. 9a that beyond 8% of volumetric moisture content, the dielectric constant decreases with increasing temperature from 40 to 90°C at the same moisture level. This decrease in dielectric constants with rising temperature at higher moisture content levels could be attributed to Debye relaxation behaviour. As the temperature rises, the relaxation time of polar molecules (water) decreases due to enhanced molecular mobility (Gezahegn et al. 2021; Andryieuski et al. 2015). This shift moves the relaxation peak to higher frequencies, resulting in a reduced ε_r' at the fixed frequency of 2.45 GHz. However, at lower moisture contents, the dielectric constants within the temperature range from room temperature (~20 °C) to 80 °C did not show substantial differences with varying temperatures. This stability is likely due to the dominance of bound water, whose restricted molecular movement leads to relatively consistent dielectric constants across different temperatures. Additionally, the dielectric constant of UGM at 90°C was the lowest among the measured values across all moisture levels. This could be due to increased thermal energy at higher temperatures, leading to lower dielectric constants, or it may reflect measurement inaccuracies at these elevated temperatures. Given the increased thermal variability observed at 90 °C (Sect. 2.3), these measurements carry higher uncertainty and should be interpreted with caution.

To further interpret the observed trends, the applicability of a dielectric mixing model for predicting dielectric constant variations with volumetric moisture content and temperature was evaluated using the Birchak mixing model (Birchak et al. 1974). The

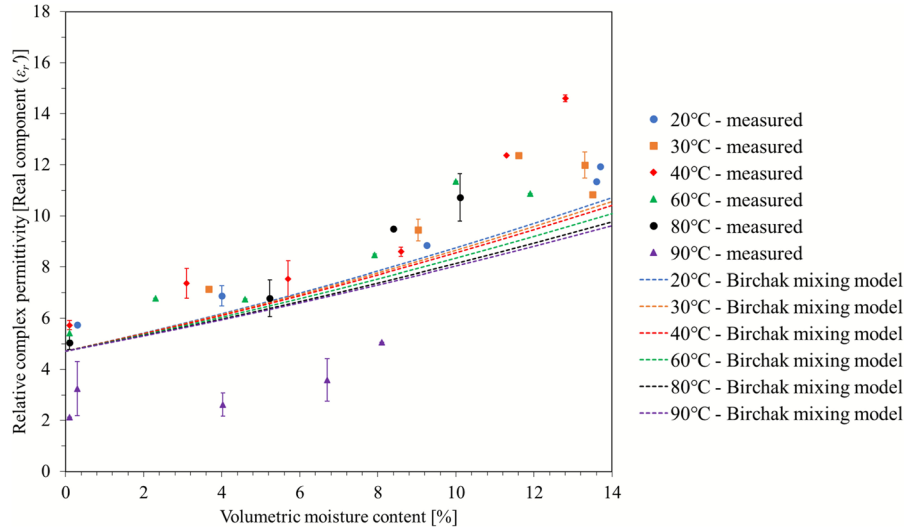

Fig. 11 Comparison of measured dielectric constants (ε_r') of Class 2 UGM with predictions from the Birchak mixing model across different volumetric moisture contents and temperatures

Table 9 Fitted values of the Birchak mixing model parameter α for the tested UGM at different temperatures

Temperature (°C)	Fitted α value	R^2
20	0.63	0.97
30	0.72	0.79
40	0.90	0.88
60	0.83	0.90
80	0.89	0.95

Birchak mixing model estimates the effective dielectric constant of a mixture by considering the volume fractions and dielectric properties of its components (Birchak et al. 1974). It is expressed as.

$$\varepsilon_{eff}^{\alpha} = \sum_{i=1}^{n} v_i \varepsilon_i^{\alpha} \tag{6}$$

where ε_{eff} is the effective dielectric constant of the mixture, v_i is the volume fraction of the i^{th} component, ε_i is the dielectric constant of the i^{th} component, and α is an empirical parameter typically set to 0.5 for many soils (Dobson et al. 1985; Orangi 2019). Figure 11 illustrates the comparison between the experimentally measured dielectric constants and the predictions from the Birchak mixing model, which incorporates temperature-dependent dielectric constants for free water. The Birchak mixing model demonstrates a consistent decline in dielectric constant with increasing temperature at a given VMC, reflecting the well-established reduction in the polarisability of water molecules at elevated temperatures. It also predicts negligible temperature sensitivity at low moisture contents (VMC < 4%), where the contribution of water to the effective permittivity is minimal. A comparable trend was observed in the experimental data, wherein the dielectric constant values remained relatively close across all temperatures at low VMC. However, notable deviations from the model were observed at higher moisture contents. Specifically, the measured permittivity values at 20 °C and 30 °C were lower than those recorded at 40 °C, 60 °C and 80 °C, contrary to the expected monotonic trend. In addition, the measurements at 90 °C were substantially lower than the corresponding model predictions, whereas values at intermediate temperatures generally exceeded those predicted by the Birchak mixing model. These discrepancies are likely attributed to the simplified nature of the Birchak mixing model, which assumed a three-phase system consisting of air, free water, and solids, and did not account for the bound water. Given that the dielectric behaviour of bound water is influenced by its local molecular environment (i.e., adsorption forces, temperature variations, and surface interactions) and is not easily quantified, its omission may contribute to the observed inconsistencies. In addition, the power value α in the Birchak mixing model is a material-specific parameter, and its assumed value of 0.5 may not accurately represent the dielectric behaviour of the compacted UGM used in this study (Orangi et al. 2020). This could be another contributing factor to the deviations observed between the measured and modelled dielectric constant values. Other influencing factors may include thermal gradients, moisture redistribution, and increased measurement uncertainty at elevated temperatures.

To further examine the deviations observed between the measured dielectric constants and the Birchak mixing model predictions with $\alpha = 0.5$ (Fig. 11), a quick fitting analysis was conducted for each temperature. Table 9 summarises the fitted α values for the Birchak mixing model and corresponding R^2 values for the tested UGM at different temperatures. The resulting α values ranged from 0.63 to 0.9 for temperatures up to 80 °C, with generally high R^2 values (> 0.8), indicating a good agreement between the model and measurements. At 90 °C, substantial scatter and deviation from the model prevented reliable fitting, likely due to increased measurement uncertainty at elevated temperatures. The systematic departure of α from 0.5 can be interpreted as an empirical adjustment compensating for microstructural features of compacted UGM that are not explicitly represented in the simplified three-phase model. In compacted UGM, the dense granular skeleton and fines content create a heterogeneous structure in which a portion of the water is expected to exist as thin, surface-bound films at low VMC and gradually transition to free water as VMC increases. Because the permittivity and volumetric fraction of bound water cannot be readily quantified, both bound and free water were treated as a single phase in this study. Under this simplification, the fitted α implicitly accounts for the reduced dielectric contribution of bound water in the mixture. The temperature

dependence of the fitted α values further suggests that α is temperature-dependent for the tested UGM. Increasing temperature weakens hydration forces, thins bound-water layers, increases molecular mobility, and reduces the dielectric constant of free water, collectively influencing the effective mixture response. The results also highlight the limitations of representing the UGM–air–water system using a simple three-phase formulation. A four-phase conceptual approach that distinguishes bound water from free water, in addition to the solid and air phases, may provide a more physically realistic representation of the dielectric behaviour of the compacted UGM. Future work may therefore consider developing or applying mixing models that explicitly incorporate bound-water behaviour and temperature dependence to improve physical realism and predictive accuracy.

The dielectric loss or imaginary component (ε_r'') decreases with increasing volumetric moisture contents across all temperatures, as shown in Fig. 9b. Water molecules are bound to the material's surface at lower moisture contents and exhibit significant relaxation losses, contributing to higher dielectric loss. As moisture content increases, the proportion of free water molecules increases. Free water has a lower dielectric loss compared to bound water because the free water molecules can reorient more freely under an alternating electric field without as much energy loss (Abdulraheem et al. 2024; Chauhan et al. 2024). Similar to dielectric constant variation, the dielectric loss of UGM decreases with increasing temperature. This observation is consistent across all temperatures from room temperature (~ 20 °C) to 90 °C. At higher temperatures, reduced dipolar rotation of water molecules due to thermal agitation decreases friction between dipolar molecules and reduces dielectric loss (Vijay et al. 2015).

In contrast to the observed variation in dielectric constants at lower moisture levels, dielectric losses show a noticeable difference between the various temperatures, with the highest losses occurring at room temperature. It can also be seen from Fig. 9 that both dielectric constant and dielectric loss show minimal variation with increasing moisture content up to 8% of VMC. This could be due to the limited mobility of bound water molecules at lower moisture contents, which results in relatively stable dielectric properties of UGM across all temperatures.

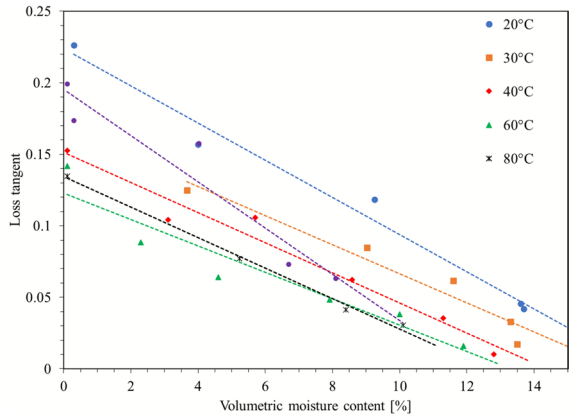

Fig. 12 Loss tangent of Class 2 UGM at 2.45 GHz frequency with varying volumetric moisture contents and temperatures

The increasing trend of dielectric constant with moisture content is well-documented and aligns with previous studies (Kishore 2023; Muller and Scheuermann 2016; Cihlar and Ulaby 1974). However, the observed decrease in dielectric loss with increasing moisture content is unusual and not commonly reported in the literature. Several mechanisms may have contributed to this atypical behaviour. Typically, dielectric loss is expected to increase with moisture content due to the greater presence of free water, which generally contributes to higher energy dissipation. As discussed previously, the observed decrease could be attributed to the transition from bound water to free water within the material's structure. The gradual drying process during sample preparation might have caused structural changes (e.g., moisture redistribution and slight variations in porosity) in the compacted UGM sample, which might have influenced the variation of dielectric loss with moisture content. Moreover, it is crucial to consider potential errors during measurement. Rapid changes in temperature during the measurements, especially at elevated temperatures, might have influenced the observed trend. In addition, experimental artefacts such as potential internal reflections or from surroundings, small air gaps or inconsistencies in the experimental setup, may have contributed to the unexpected decrease in dielectric loss of UGM at 2.45 GHz frequency (Muller and Dérobert 2013).

In summary, the regression model for Class 2 UGM at 2.45 GHz, incorporating temperature-dependent coefficients, provided a comprehensive and

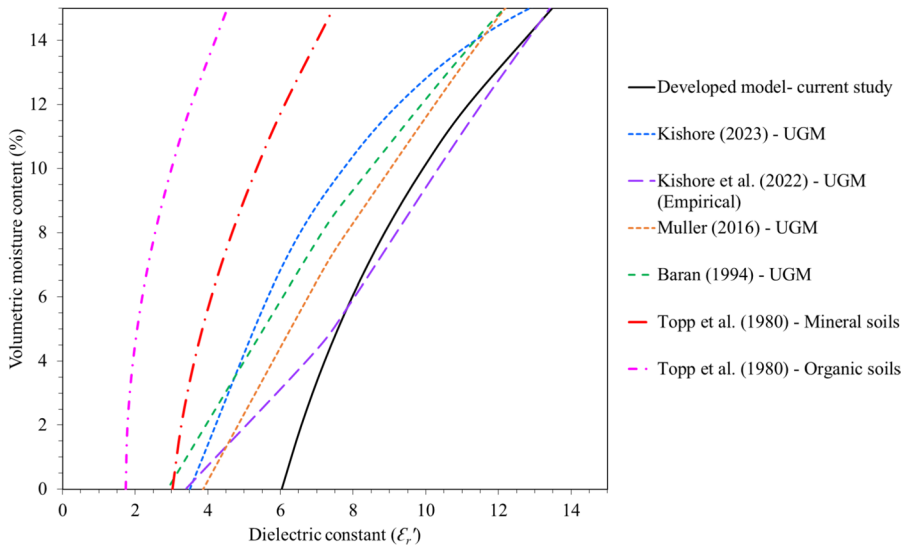

Fig. 13 Comparison of the developed dielectric constant model (ε_r') with existing permittivity models for different soils and UGMs at room temperature (UGM – unbound granular materials)

Table 10 Error statistics for different permittivity models [MAE – mean absolute error, RMSE – root mean square error]

Model	MAE [%]	RMSE [%]
Topp et al. (1980) – Mineral soils	12.2	12.6
Topp et al. (1980) – Organic soils	19.1	19.2
Baran (1994) – UGM	2.1	2.4
Muller (2016) – UGM	3.5	3.9
Kishore et al. (2022) – UGM (Empirical)	1.5	2.8
Kishore (2023) – UGM	4.2	4.6

good prediction of dielectric properties across a range of volumetric moisture contents and temperatures. This approach simplified the analysis and enhanced the model's applicability for practical implementations, such as numerical simulations and optimisation of microwave drying processes.

3.3 Loss Tangent of UGM at 2.45 GHz Frequency

The loss tangent ($\tan\delta$) is defined as the ratio of the dielectric loss and dielectric constant according to

$$\tan\delta = \frac{\varepsilon_r''}{\varepsilon_r'} \tag{7}$$

where δ is the phase angle. The loss tangent indicates the capability of the material to convert the microwave energy into heat (Pongsuwan et al. 2014). This parameter is particularly important for evaluating the heating efficiency of materials exposed to microwave energy, making it a critical factor in optimising microwave drying performance for civil engineering applications (Barba and D'Amore 2012).

Figure 12 illustrates the variation of the loss tangent of the selected UGM at 2.45 GHz across different moisture contents and temperatures. The data points represent the calculated loss tangent values, while the dashed lines indicate the best-fit lines developed for the measured data at each temperature to illustrate the overall trend. The loss tangents decreased with increasing moisture content and temperature. Further, the calculated loss tangents show a negative linear relationship with moisture content at each temperature. This observation may be due to the transition of bound water to free water, leading to a negative correlation between loss tangent and moisture content. Alternatively, it could be attributed to potential measurement errors during the experiments. Moreover, it can be observed that the loss tangent values decrease with increasing temperature at a given moisture level (except at 90^0C). Overall, the loss tangent decreased with both VMC and temperature, indicating reduced energy dissipation at higher temperatures. This may also imply slower volumetric heating compared to lower temperatures, though further heating-rate experiments are required to verify this behaviour. Future studies should investigate whether these changes influence the uniformity and efficiency of microwave heating in UGM.

3.4 Comparison of the Developed Dielectric Constant Model with Existing Permittivity Models

As discussed, existing complex permittivity models for GPR and TDR have been primarily developed for moisture measurements at room temperature. These models often neglect the dielectric loss due to its relatively small magnitude compared to the dielectric constant. Moreover, none of the current models consider the combined effects of both moisture content and temperature variations. Therefore, the dielectric constant model developed at room temperature was compared in Fig. 13 with existing complex permittivity models developed for UGMs or pavement materials, along with the widely used Topp model for different soil types, which serves as a general benchmark for moisture content estimation in current practice. To support the comparison between the developed model and previous permittivity models, a quantitative error evaluation was performed. Table 10 summarises the MAE and RMSE for each model across the tested VMC range.

The developed model in this study and other existing permittivity models show a consistent trend of increasing dielectric constant with increasing

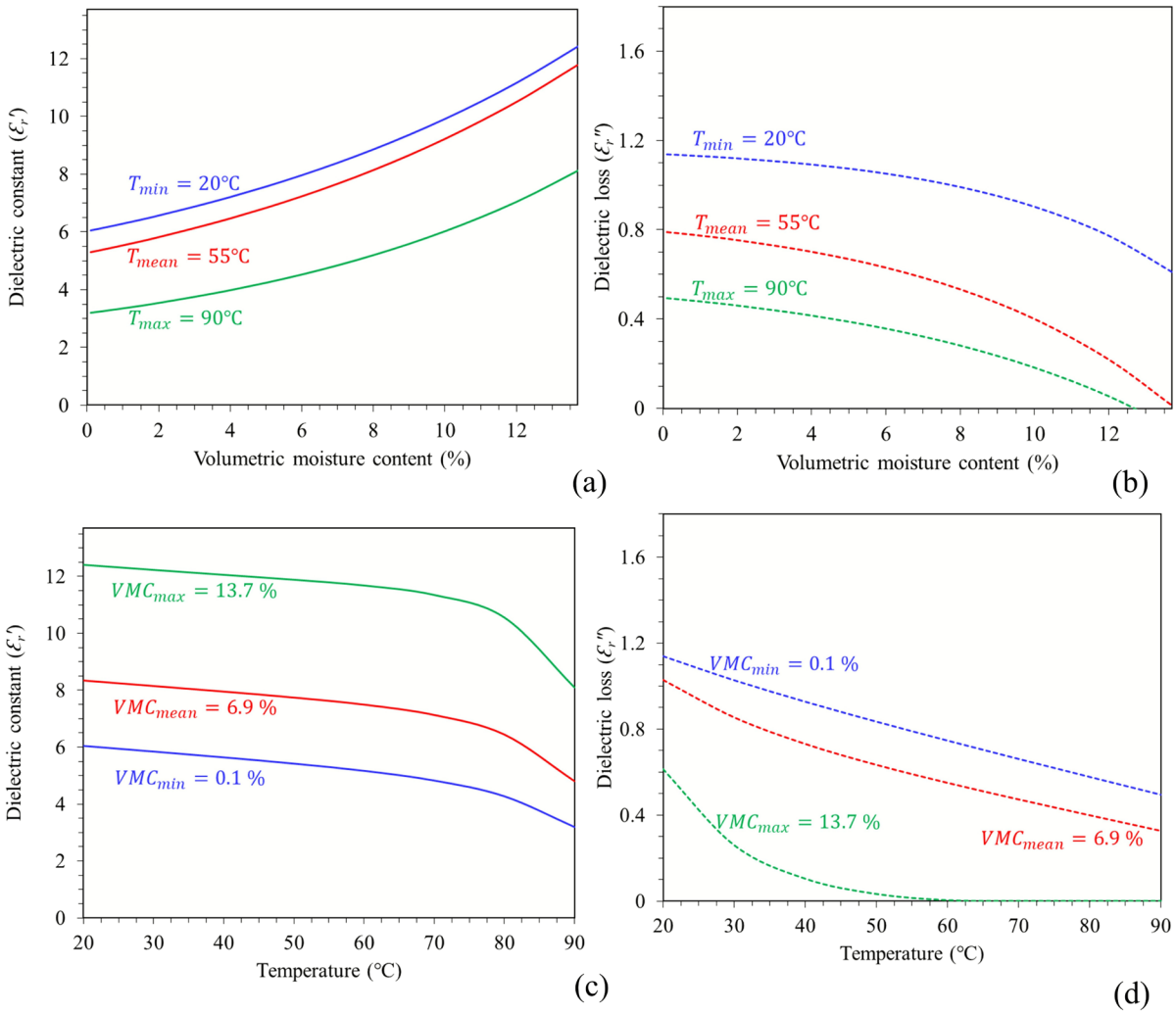

Fig. 14 Parametric study showing the variation of complex permittivity with respect to different variables: **a** dielectric constant variation with volumetric moisture content, **b** dielectric loss variation with volumetric moisture content, **c** dielectric constant variation with temperature, and **d** dielectric loss variation with temperature

Table 11 Summary of input variables for Variable Importance Analysis

Input variable	Number of data points	Mean	Minimum	Maximum
Temperature (°C)	31	55	20	90
VMC (%)	31	6.9	0.1	13.7

moisture content. However, Fig. 13 indicates that the existing permittivity models are material-specific and overestimate the moisture content when applied to Class 2 UGM used in this study. For instance, Topp's model for mineral and organic soils substantially overestimates the VMC (MAE 12.2 -19.1%; RMSE 12.6—19.2%), mainly due to the fundamental difference between the uncompacted soils and compacted UGMs. Models developed for UGMs show lower errors but still exhibit systematic deviations. The models by Baran (1994) and Muller (2016) yield MAE values of 2.1–3.5%, which may be attributed to differences in aggregate mineralogy, fines content, grading, compaction state, and measurement approaches. The empirical model proposed by Kishore et al. (2022), also developed using modified free-space transmission technique, provides the closest agreement (MAE = 1.5%), where some deviations were observed at low moisture content (VMC ≤ 5%).

Overall, the model developed in this study was calibrated specifically for Class 2 UGM compacted under controlled laboratory conditions. Variability in material composition (e.g., sand and clay content, particle shape, fines content) and possible measurement uncertainties may explain the differences observed relative to existing models. While the existing empirical models and the current model in this study perform well for the materials and conditions for which they were developed, their direct application to other soils or UGMs without calibration may reduce accuracy. Additionally, the developed model's incorporation of varying moisture content and temperature effects makes it a valuable tool for assessing the microwave drying behaviour of the UGM in the current research context.

3.5 Parametric Study and Sensitivity Analysis

A parametric study was performed to explore how variations in specific parameters influence the behaviour of the developed permittivity model. The analysis involved altering one input variable at a time while keeping the others fixed at their average values (Kiani et al. 2016). The parametric study results depicted in Fig. 14 show that with an increase in VMC, there is a consistent rise in the dielectric constant of the UGM. Conversely, the dielectric loss of the UGM decreased with increasing VMC, as shown in Fig. 14b. In addition, both dielectric constant and dielectric loss of the UGM decreased with an increase in temperature, following a non-linear trend. However, dielectric loss exhibited a pronounced drop with increasing temperature compared to the dielectric constant. Notably, the dielectric constant indicated a sharp drop beyond 80 °C (Fig. 14c), indicating possible changes in material behaviour at higher temperatures.

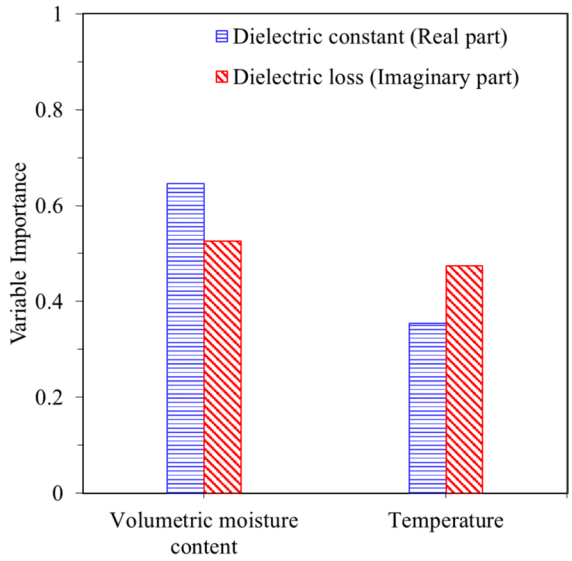

Fig. 15 Sensitivity analysis of each input variable on the variation of complex permittivity of the selected UGM

Sensitivity analysis also referred to as Variable Importance (VI), was then employed to quantify the effect of each input variable on the model's output. This analysis helped to understand the influence of individual features on the predictive performance of the developed permittivity model. In this study, the sensitivity of each parameter (i) was evaluated by examining the change in model output (L_i) when the input parameter was varied from its maximum (i_{max}) to its minimum (i_{min}) value, while the other input parameters were kept constant at their mean

values [Eq. (8)] (Tophel et al. 2023, 2025; Kiani et al. 2016). The VI was calculated as the percentage of each obtained output difference for each parameter, as shown in

$$L_i = \left| f(i_{max}) - f(i_{min}) \right| \tag{8}$$

$$\mathrm{VI} = \frac{L_i}{\sum_{j=1}^{j=n} L_j} \tag{9}$$

where the minimum, maximum, and mean values of each input parameter used in this analysis are summarised in Table 11. The minimum, maximum, and mean values in Table 11 represent the range of the experimental measurements, which also define the input data range for the developed model. Using these ranges, a sensitivity analysis was performed to assess the influence of each parameter on the predicted complex permittivity of Class 2 UGM, as presented in Fig. 15. The analysis reveals that VMC is the most significant factor influencing both the dielectric constant and dielectric loss of the selected UGM. Specifically, the impact of VMC on the dielectric constant was notably high, with a variable importance (VI) value of 0.65. In contrast, the effect of temperature on the dielectric constant, with a VI of 0.35, was considerably lower, indicating a substantial difference in their respective influences. Additionally, the influence of VMC and temperature on dielectric loss was nearly comparable, with VI values of 0.53 and 0.47, respectively. In summary, both the parametric study and variable importance analysis confirmed that VMC is the predominant factor affecting the dielectric properties of the UGM, particularly the dielectric constant. At the same time, temperature also plays a substantial role, especially in influencing the dielectric loss.

4 Conclusions

This paper presented the experimental characterisation and empirical modelling of the complex permittivity of Class 2 unbound granular material (UGM) as a function of volumetric moisture content (VMC) and temperature at 2.45 GHz.

Key findings highlighted that both parameters significantly influence the dielectric constant and dielectric loss, with VMC emerging as the most dominant factor. An increase in VMC led to a consistent rise in the dielectric constant, enhancing the material's capacity to store energy. Conversely, the dielectric loss decreased with increasing VMC, indicating reduced energy dissipation. Temperature also had a substantial impact, particularly on dielectric loss. Increased temperature resulted in a notable reduction in dielectric loss, likely due to decreased dipolar relaxation and reorientation of water molecules within the material. Moreover, while the dielectric constant showed an expected increase with rising VMC, the dielectric loss exhibited an unusual decline with increasing moisture content- a trend not commonly reported in past studies. This uncharacteristic behaviour may be attributed to structural changes during the drying process of the compacted UGM, and potential measurement errors might have contributed to this trend. Moreover, at 90℃, the measurements exhibited increased variability, consistent with the higher thermal differences observed at this temperature. Therefore, the dielectric properties at 90 °C carry greater uncertainty and should be interpreted with caution. Minor variability may also arise from the use of tap water, due to the dissolved ionic content, and these aspects warrant further investigation.

Additionally, the measured dielectric constants were compared with predictions from the Birchak mixing model. While general agreement was found at lower VMCs, substantial deviations occurred at higher moisture levels and elevated temperatures. These differences may stem from the model's simplified three-phase assumption (air, solid, and free water) and its fixed exponent $\alpha = 0.5$, which may not accurately represent the dielectric behaviour of compacted UGM. A separate fitting analysis in this study yielded α values ranging from 0.63 to 0.90 for temperatures up to 80 °C, confirming that α is both material and temperature dependent.

Comparing the developed permittivity model with existing models developed for different soils and UGMs revealed similar trends with increasing moisture contents. However, deviations in the predicted dielectric constant in this study, compared to existing permittivity models, could be attributed to differences in material characteristics, compaction level, and experimental setup. Alternatively, the potential measurement error due to interference by reflections from the surroundings during experiments may have

contributed to higher predictions of relative permittivity values.

Overall, the developed permittivity model, which incorporates the combined effects of VMC and temperature, provides a practical tool for designing and optimising microwave dry-back systems for compacted granular pavement layers. By predicting the dielectric behaviour of the tested UGM, the model can be directly integrated into numerical simulations to assess drying performance, estimate energy requirements, and optimise operational parameters such as power level, exposure time, and antenna configuration. In addition, the developed model is valuable for predicting drying efficiency and depth during these stages, supporting informed decisions for equipment design, process control, and field implementation.

While the developed model and analysis provide a comprehensive understanding of the dielectric behaviour of UGM under controlled laboratory conditions, future work should focus on validating these relationships under broader moisture and temperature ranges. Expanding the experimental scope to include additional material types would further enhance the model's general applicability. Future research could also explore the coupled influences of frequency, density, and microstructural characteristics on dielectric response to improve predictive accuracy. In particular, further work is required to validate dielectric behaviour at elevated temperatures, where the increased thermal variability observed in this study highlights the need for improved measurement reliability across the full thermal range relevant to microwave applications. Finally, integrating the developed model into coupled heat and moisture transfer simulations will support the optimisation of microwave-based drying systems for practical road construction applications.

Acknowledgements This research was part of a project (Project number: IH18.03.8) sponsored by the SPARC Hub (https://sparchub.org.au) within the Department of Civil and Environmental Engineering, Monash University, funded by the Australian Research Council (ARC) Industrial Transformation Research Hub (ITRH) Scheme (Project ID: IH180100010). The authors would like to thank the technical staff in the Department of Civil and Environmental Engineering, Monash University for their help in supporting the experiment. The authors would also like to thank the Smart Pavements Australia Research Collaboration (SPARC) Hub, Construction, Infrastructure, Mining and Concessions (CIMIC), and Engineering, Innovation and Capability (EIC) activities for their financial support, and SPARC Hub members for their moral support throughout the experiments.

Funding This study was supported by the Australian Research Council (ARC) Industrial Transformation Research Hub (ITRH) Scheme (Grant No. IH180100010).

Data Availability The data that support the findings of this study are available upon reasonable request.

Declarations

Competing interests The authors declare that they have no known competing financial interests or personal relationships that could have appeared to influence the work reported in this paper.

Appendix A

Calibration Results

The permittivity values of water and Teflon were measured using a modified free-space transmission measurement technique to validate the experimental setup and ascertain the stable measurement range of frequency. Figures 16 and 17 illustrate the variations in the real and imaginary components of the complex permittivity of these calibration materials across the frequency range of 300 kHz to 4.5 GHz.

In Fig. 16a, the dielectric constants (ε_r') of water and Teflon are plotted against frequency. At lower frequencies, specifically from 300 to 500 kHz, both materials exhibited higher permittivity values, with water surpassing the anticipated value of 80 and Teflon exceeding 2.1. This discrepancy is attributed to the polarisation effects of dipolar molecules and potential measurement noise at these lower frequencies. The dipolar nature of water molecules allows them to align with the electric field more effectively and respond more readily to changes in the electric field. This increased ability to polarise at lower frequencies resulted in higher values of permittivity, as the molecules require less energy to align with the electric field. Consequently, ε_r' is elevated at these lower frequencies (Debye 1929; Kishore 2023). As the frequency was increased, the permittivity values stabilised, approaching the known values of 80 for

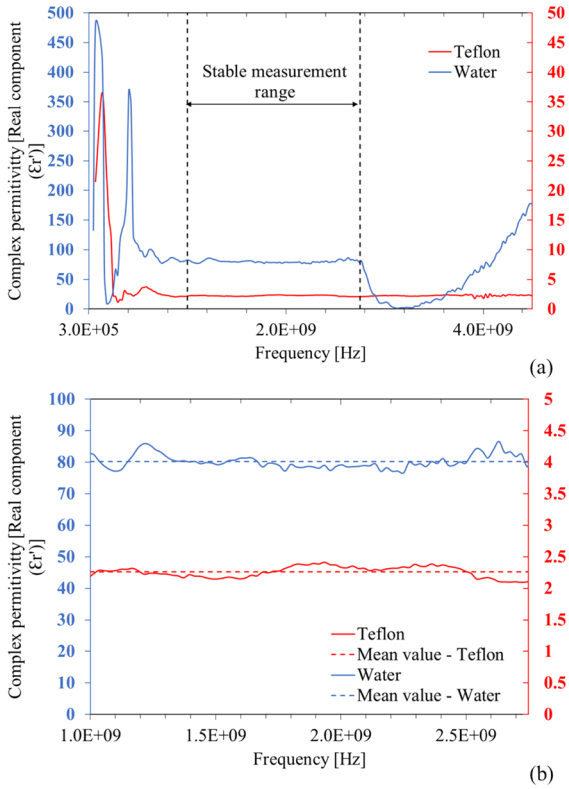

Fig. 16 Real component of complex permittivity for calibration measurements using modified free space transmission measurement technique, **a** Variations in dielectric constants of water and Teflon across the frequency spectrum, and **b** Variations in dielectric constant of calibration materials within the selected stable frequency measurement range

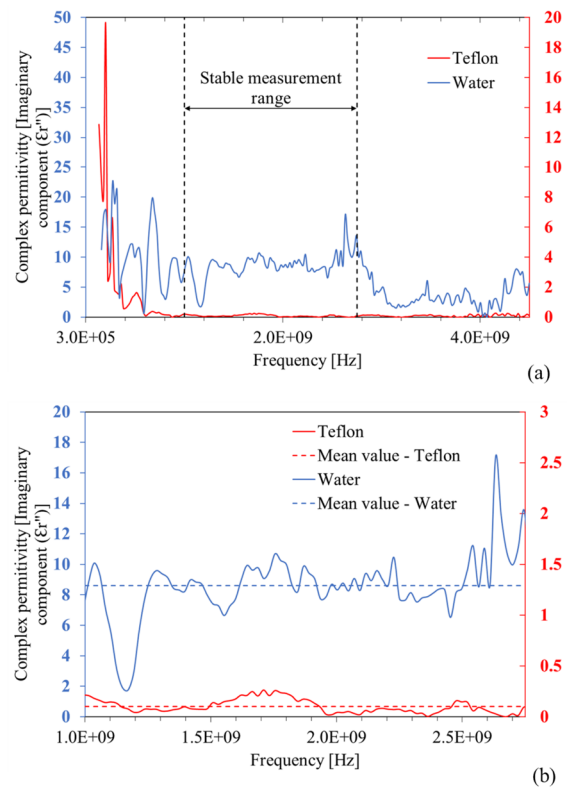

Fig. 17 Imaginary component of complex permittivity for calibration measurements using modified free space transmission measurement technique, **a** Variations in dielectric loss of water and Teflon across the frequency spectrum, and **b** Variations in dielectric loss of calibration materials within selected stable frequency measurement range

water and 2.1 for Teflon within the frequency range of 1–4.5 GHz.

It can be seen from Fig. 16a that there is a drop in the real component of complex permittivity of water from the anticipated value of 80 after 2.75 GHz. Water exhibits dielectric relaxation, a process where the polarisation of the water molecules cannot keep up with the rapidly changing electric field at higher frequencies. The primary relaxation frequency of water is around 17 GHz, but the effects start becoming significant at frequencies above a few GHz (Kaatze 2015). As the frequency increases, the ability of water molecules to orient themselves in response to the alternating field diminishes, leading to a decrease in ε_r' (Frohlich 1958). In addition, there may be limitations in the measurement setup or calibration accuracy at higher frequencies, leading to inconsistencies in the measured permittivity values. Overall, the measured dielectric constant of both water and Teflon was within the desired range (Mean values for water and Teflon are respectively 80.2 and 2.3) in the frequency range of 1 GHz to 2.75 GHz (Fig. 16b), indicating the reliability of the measurement setup in this frequency band.

Figure 17a presents the variation of dielectric loss (ε_r'') for water and Teflon. Similar to the real component, the imaginary component of permittivity values is higher than expected at lower frequencies, reflecting increased dielectric losses. As the frequency is increased, ε_r'' values decrease and align more closely with theoretical expectations, particularly in the range of 1 GHz to 2.75 GHz. This trend further substantiates the effectiveness of the measurement setup in this higher frequency range.

Figures 16b and 17b emphasise the permittivity values within the selected stable measurement range

(1–2.75 GHz). Within this range, both the real and imaginary components of the permittivity of water and Teflon remain consistent with the known values, indicating minimal measurement distortion and reliable data acquisition. This validation confirmed that the modified free-space transmission technique was robust and accurate for the frequency range from 1 to 2.75 GHz.

The calibration process is crucial for ensuring the reliability of subsequent measurements of the selected UGM. By establishing a stable measurement range and validating the setup with materials of known permittivity, the accuracy of the complex permittivity data for the UGM can be confidently assessed. This procedure forms a foundation for further analysis of the UGM's dielectric properties as a function of temperature and moisture content, which is essential for understanding their behaviour under various applications (e.g., microwave treatment).

References

Abdulraheem MI, Chen H, Li L et al (2024) Recent advances in dielectric properties-based soil water content measurements. Remote Sens. https://doi.org/10.3390/rs16081328

Ali SZ, Ahsan K, ul Khairi D et al (2024) Advancements in FR4 dielectric analysis: free space approach and measurement validation. PLoS ONE 19(9):e0305614

Andryieuski A, Kuznetsova SM, Zhukovsky SV et al (2015) Water: promising opportunities for tunable all-dielectric electromagnetic metamaterials. Sci Rep 5:13535

AS-1289.3.1.1 (2009) Soil classification tests - Determination of the liquid limit of a soil- Four point casagrande method. Standards Australia.

AS-1289.3.5.1 (2006) Methods of testing soils for engineering purposes - Soil classification tests - Determination of the soil particle density of a soil - Standard method. Standards Australia.

AS-1289.3.6.1 (2009) Methods of testing soils for engineering purposes - Soil classification tests - Determination of the particle size distribution of a soil - Standard method of analysis by sieving. Standards Australia.

AS-1289.5.2.1 (2017) Methods of testing soils for engineering purposes - Soil compaction and density tests - Determination of the dry density/moisture content relation of a soil using modified compactive effort. Sydney: Standards Australia.

Asha MN, Suku L, Babu GLS (2025) Shakedown analysis of granular sub-base behaviour. Geotech Geol Eng 43(3):128

Athmarajah G, Walker JP, Sounthararajah A et al. (2023) Influence of solar energy on the dry back process in road pavement construction: an experimental study. XXVII PIARC World Road Congress, 11.

Athmarajah G, Sounthararajah A, Walker JP et al (2024) An alternative technology using microwaves for dry back process of unbound granular pavements during construction – a review. Transp Geotech. https://doi.org/10.1016/j.trgeo.2024.101245

Athmarajah G (2025) Microwave dry-back of granular pavement layers. (Doctor of Philosophy). Monash University.

Athmarajah G, Walker J, Chen L et al. (2025) Microwave dry-back of compacted unbound granular materials - An experimental and numerical study. Géotechnique.

Austroads (2008) Guide to Pavement Technology Part 4A: Granular Base and Subbase Materials, AGPT04A-08. Sydney NSW 2000 Australia: Austroads Ltd.

Azoor RM, Deo RN, Birbilis N et al (2019) On the optimum soil moisture for underground corrosion in different soil types. Corros Sci. https://doi.org/10.1016/j.corsci.2019.108116

Baran E (1994) Use of time domain reflectometry for monitoring moisture changes in crushed rock pavements. In: Proceeding of the Symposium: Time-Domain Reflectomerty in Environmental, Infrastructure, and Mining Applications, 349–356.

Barba AA, D'Amore M 2012 Relevance of Dielectric Properties in Microwave Assisted Processes. In: Costanzo, S. ed. Microwave Materials Characterization. Rijeka: IntechOpen.

Birchak JR, Gardner CG, Hipp JE et al (1974) High dielectric constant microwave probes for sensing soil moisture. Proc IEEE 62(1):93–98

Bircher S, Demontoux F, Razafindratsima S et al (2016) L-Band relative permittivity of organic soil surface layers—a new dataset of resonant cavity measurements and model evaluation. Remote Sens. https://doi.org/10.3390/rs8121024

Chauhan PD, Gadani DH, Rana VA (2024) Effect of moisture content variation on dielectric properties of various plant leaves at microwave frequencies. Sci Rep 14(1):13204

Cihlar J, Ulaby FT 1974 Dielectric Properties of Soils as a Function of Moisture content. National Aeronautics and Space Administration, 177–47.

Debye PJW (1929) Polar Molecules. Dover Publications, New York

Dobson MC, Ulaby FT, Hallikainen MT et al (1985) Microwave dielectric behavior of wet soil-part II: dielectric mixing models. IEEE Trans Geosci Remote Sens 23:12

Du E, Zhao L, Hu G et al (2025) A soil refractive index (SRI) model characterizing the functional relationship between soil moisture content and permittivity. Water 17(3):399

Dushmantha A, Gallage C (2025) During- and post-flood damage-vulnerability window in unbound granular pavements: a degree-of-saturation threshold decision rule. Results Eng 28:108157

Dutta TT, Tophel A, Kodikara J 2024 Resilient and rutting response of unbound granular material and subgrade soil influenced by initial state and stress conditions. Road Materials and Pavement Design, pp 1–33.

Ekblad J, Isacsson U (2007) Time-domain reflectometry measurements and soil-water characteristic curves of coarse granular materials used in road pavements. Can Geotech J 44(7):858–872

Fazel Mojtahedi SF, Akbarpour A, Darzi AG et al (2024) Prediction of stress-dependent soil water retention using machine learning. Geotech Geol Eng 42(5):3939–3966
Fredlund DG (2006) Unsaturated soil mechanics in engineering practice. J Geotech Geoenviron Eng 132(3):286–321
Frohlich H 1958 Theory of Dielectrics: Dielectric Constant and Dielectric Loss. Oxford University Press.
Gdeisat M, Lilley F (2011) One-dimensional phase unwrapping problem. Signal 4:6
Gezahegn YA, Tang J, Sablani SS et al (2021) Dielectric properties of water relevant to microwave assisted thermal pasteurization and sterilization of packaged foods. Innov Food Sci Emerg Technol. https://doi.org/10.1016/j.ifset.2021.102837
Gulisano F, Gallego J (2021) Microwave heating of asphalt paving materials: principles, current status and next steps. Constr Build Mater. https://doi.org/10.1016/j.conbuildmat.2020.121993
Hilf JW 1956 An Investigation of Pore-Water Pressure in Compacted Cohesive Soils. ProQuest Dissertations Publishing.
Jacobsen OH, Schjonning P (1993) A laboratory calibration of time domain reflectometry for soil water measurement including effects of bulk density and texture. J Hydrol 151:147–157
Kaatze U 2015 Dielectric relaxation of water. Dielectric relaxation in biological systems: physical principles, methods, and applications. Oxford University Press, Oxford, UK, 189–227.
Kabir H, Khan MJ, Brodie G et al (2020) Measurement and modelling of soil dielectric properties as a function of soil class and moisture content. J Microw Power Electromagn Energy 54(1):3–18
Kaplan ST, Ulrych TJ 2007 Phase Unwrapping: A Review of Methods and a Novel Technique. Let it Flow – 2007 CSPG CSEG Convention. 534–537.
Keysight Technologies (2021) Specifying calibration standards and kits for Keysight vector network analyzers.
Khan MJ, Brodie G, Gupta D (2019) Potential of microwave soil heating for weed management and yield improvement in rice cropping. Crop Pasture Sci 70(3):211–217
Kiani B, Gandomi AH, Sajedi S et al (2016) New formulation of compressive strength of preformed-foam cellular concrete: an evolutionary approach. J Mater Civ Eng 28(10):04016092
Kishore K, Singh N, Deo R et al. (2022) Moisture-permittivity relationship of unbound granular materials for GPR application. In: 19th International Conference on Ground Penetrating Radar. 55–58.
Kishore KK (2023) The development of quantitative moisture monitoring methods for intelligent soil compaction using ground penetrating radar. (Doctor of Philosophy). Monash University.
Kodikara J (2012) New framework for volumetric constitutive behaviour of compacted unsaturated soils. Can Geotech J 49(11):1227–1243
Kumar C, Joardder MUH, Farrell TW et al (2017) Investigation of intermittent microwave convective drying (IMCD) of food materials by a coupled 3D electromagnetics and multiphase model. Drying Technol 36(6):736–750
Malicki MA, Plagge R, Roth CH (1996) Improving the calibration of dielectric TDR soil moisture determination taking into account the solid soil. Eur J Soil Sci 47(3):357–366
Metaxas AC, Meredith RJ (1983) Industrial microwave heating. The Institution of Engineering and Technology, London, United Kingdom
Midgley L (2008) Technical Report TR 207 Ingredients of an Unbound Granular Pavement for a Successful Sprayed Seal 1st Sprayed Sealing Conference - cost effective high performance surfacings.
Muller WB (2016) Permittivity characterization of unbound granular pavement materials with a modified free-space approach. Transp Res Rec J Transp Res Board 2578(1):93–101
Muller W, Dérobert X (2013) A comparison of phase-shift and one-port coaxial cell permittivity measurements for GPR applications. In: 2013 7th International Workshop on Advanced Ground Penetrating Radar, 2013, 1–6.
Muller W, Scheuermann A (2016) Optimising a modified free-space permittivity characterisation method for civil engineering applications. J Geophys Eng 13(2):S9–S18
Müller W, Schuermann A, Reeves B (2012) Quantitative moisture measurement of road pavements using 3D noise-modulated GPR. In: 2012 14th International Conference on Ground Penetrating Radar (GPR), 2012, 517–523.
Nelson SO (1991) Dielectric properties of agricultural products-measurements and applications. IEEE Trans Electr Insul. https://doi.org/10.1109/14.99097
Orangi A (2019) Evaluation of Soil Parameters Using Dielectric Permittivity. (Doctor of Philosophy). The University of Melbourne.
Orangi A, Narsilio GA, Wang YH et al (2020) Experimental investigation of dry density effects on dielectric properties of soil–water mixtures with different specific surface areas. Acta Geotech 15(5):1153–1172
Palta P, Kaur P, Mann KS (2022) Dielectric behavior of soil as a function of frequency, temperature, moisture content and soil texture: a deep neural networks based regression model. J Microw Power Electromagn Energy 56(3):145–167
Pepin S, Livingston NJ, Hook WR (1995) Temperature-dependent measurement errors in time domain reflectometry determinations of soil water. Soil Sci Soc Am J. https://doi.org/10.2136/sssaj1995.03615995005900010006x
Pongsuwan K, Pamornnak B, Chongcheawchamnan M (2014) Complex permittivity of fully ripe Palm fruit and its application for microwave heating. IEEE Trans Dielectr Electr Insul. https://doi.org/10.1109/TDEI.2014.6832290
Roth CH, Malicki MA, Plagge R (1992) Empirical evaluation of the relationship between soil dielectric constant and volumetric water content as the basis for calibrating soil moisture measurements by TDR. J Soil Sci 43:1–13
Saarenketo T (1998) Electrical properties of water in clay and silty soils. J Appl Geophys 40(1–3):73–88
Salour F 2015 Moisture Influence on Structural Behavior of Pavements. Doctoral thesis. KTH, Royal Institute of Technology,Stockholm, Sweden.
Schaap MG, de Lange L, Heimovaara TJ (1996) TDR calibration of organic forest floor media. Soil Technol 11:205–207

Sethy AK, Torgovnikov G, Vinden P et al (2015) Moisture conditioning of wood using a continuous microwave dryer. Drying Technol 34(3):318–323

Shen L, Zhu Y, Liu C et al (2020) Modelling of moving drying process and analysis of drying characteristics for germinated brown rice under continuous microwave drying. Biosyst Eng 195:64–88

Skierucha W, Walczak R, Wilczek A (2004) Comparison of open-ended coax and TDR sensors for the measurement of soil dielectric permittivity in microwave frequencies. Int Agrophys 18:355–362

Sun J, Oh E, Ong DE-L (2021) Influence of degree of saturation (DOS) on dynamic behavior of unbound granular materials. Geosciences. https://doi.org/10.3390/geosciences11020089

Taheri S, Brodie G, Jacob MV et al (2018) Dielectric properties of chickpea, red and green lentil in the microwave frequency range as a function of temperature and moisture content. J Microw Power Electromagn Energy 52(3):198–214

Tophel A, Walker J, Dutta TT et al (2022) Theory-guided machine learning to predict density evolution of sand dynamically compacted under Ko condition. Acta Geotech. https://doi.org/10.1007/s11440-021-01431-2

Tophel A, Dutta TT, Otsubo M et al (2023) Machine learning models to estimate stress wave velocities of cohesionless soils during triaxial compression influenced by particle characteristics. Soil Dyn Earthq Eng. https://doi.org/10.1016/j.soildyn.2022.107649

Tophel A, Nguyen TM, Walker JP et al (2025) Soil moisture prediction in pavement layers using LSTM neural networks. Geotech Geol Eng 43(6):318

Topp GC, Davis JL, Annan AP (1980) Electromagnetic determination of soil water content: measurements in coaxial transmission lines. Water Resour Res 16(3):574–582

Trigos L, Gallego J, Escavy JI et al (2021) Dielectric properties versus microwave heating susceptibility of aggregates for self-healing asphalt mixtures. Constr Build Mater. https://doi.org/10.1016/j.conbuildmat.2021.123475

Vergnano A, Godio A, Raffa CM et al (2020) Open-ended coaxial probe measurements of complex dielectric permittivity in diesel-contaminated soil during bioremediation. Sensors. https://doi.org/10.3390/s20226677

VicRoads (2017) Code of Practice RC 500.02 - Registration of Crushed Rock Mixes. 9.

Vijay R, Jain R, Sharma KS (2015) Dielectric properties of water at microwave frequencies. Int J Eng Res Technol (IJERT).

Wee FH, Soh PJ, Suhaizal AHM et al. (2009) Free space measurement technique on dielectric properties of agricultural residues at microwave frequencies. In: 2009 SBMO/IEEE MTT-S International Microwave and Optoelectronics Conference (IMOC), 2009, 183–187.

Yao L, Song Z, Sun C et al. 2020 Study on the evolution of internal and external water of lignite during microwave drying and the moisture reabsorption characteristics of dried lignite. Energy Sources, Part A: Recovery, Utilization, and Environmental Effects, 1–18.